UNIVERSITÀ DEGLI STUDI DI PADOVA

DIPARTIMENTO DI INGEGNERIA INDUSTRIALE

CORSO DI LAUREA MAGISTRALE IN INGEGNERIA CHIMICA E DEI PROCESSI INDUSTRIALI

Tesi di Laurea Magistrale in

Ingegneria Chimica e dei Processi Industriali

Experimental and model-based analysis for optimizing *Chromochloris zofingiensis* growth from laboratory to plant scale

Relatore: Prof. Fabrizio Bezzo

Correlatore: Dipl. Ing. Yob Ihadjadene

Correlatrice: Dipl. Ing Tehreem Syed

Laureanda: LORY ASCOLI

ANNO ACCADEMICO 2022 - 2023

Abstract

Chromochloris zofingiensis is a unicellular microalga that has attracted considerable interest due to its robust growth, its remarkable capacity to accumulate high levels of triacylglycerol and its ability to synthesize valuable keto-carotenoids including astaxanthin, one of the strongest natural antioxidants. The purpose of this thesis is to optimize the growth of *C. zofingiensis* at different scales (1L bubble column and 200L tubular reactor) by considering the main abiotic factors influencing its growth. Conventional batch experiments and photorespirometry were employed to investigate the individual effects of light intensity, temperature, nitrate and phosphate concentration and a comprehensive growth model integrating the contribution of all these factors was developed. The model expresses light as the average intensity within the culture, calculated using the Beer-Lambert law, which has been demonstrated to accurately predicts light distribution under the investigated conditions. Furthermore, the study explores the impact of oxygen accumulation, a common phenomenon in tubular reactors. Results demonstrate a significant decrease in growth rate when high levels of dissolved oxygen concentrations (DOC) are present. Additionally, it is observed that *C. zofingiensis* growth remains adversely affected if accumulation has occurred even after degassing and reducing the DOC levels, highlighting the importance of avoiding such conditions to ensure optimal growth. The initial batch experiments conducted in the 200L reactor revealed lower growth rates compared to the bubble columns, indicating possible limitations and challenges associated with implementing the laboratory-developed model in larger-scale operations. Future batches in the 200 L reactor should include monitoring of DOC levels alongside a comprehensive fluid dynamic study to gain deeper insights into the factors hindering the application of the laboratory-developed model.

Riassunto esteso

Il lavoro di tesi rappresenta il risultato di un progetto di ricerca svolto presso l'Istituto di Automazione e l'Istituto di Tecnologia dei Materiali Naturali dell'Università Tecnica di Dresda nel periodo compreso tra ottobre 2022 e aprile 2023. Lo scopo principale di questo progetto è stato lo sviluppo di un modello matematico in grado di predire la crescita della *Chromochloris zofingiensis*, tenendo in considerazione i principali fattori abiotici e le possibili implicazioni nel processo di scalabilità. La *C. zofingiensis* è un'alga verde unicellulare d'acqua dolce che ha suscitato un notevole interesse grazie alle sue caratteristiche uniche e alle sue molteplici applicazioni, tra cui la sua capacità di produrre elevati livelli di lipidi, in particolare triacilgliceroli (TAG), e l'antiossidante astaxantina. Attualmente l'applicazione industriale della *C. zofingiensis* è limitata da diverse sfide, tra cui un notevole consumo energetico, il rischio di contaminazione e altri fattori che emergono durante il processo di scaling-up da una scala di laboratorio a una scala industriale. Per superare tali ostacoli, l'utilizzo di modelli matematici riveste un ruolo cruciale nella previsione e nell'ottimizzazione del tasso di crescita delle microalghe, dimostrandosi fondamentale per valutare la redditività e la sostenibilità della coltivazione di alghe su larga scala. Tra i fattori chiave che influenzano la crescita, la luce riveste un ruolo di primaria importanza. All'interno di un sistema di coltivazione, la distribuzione della luce non è omogenea, pertanto la prima fase dello studio si è concentrata sulla modellazione di tale distribuzione e sulla definizione di una luce media da includere nel modello matematico finale. Successivamente, l'effetto dell'intensità luminosa, della temperatura e delle concentrazioni di nitrato e fosfato è stato analizzato in laboratorio attraverso esperimenti batch convenzionali e l'utilizzo della fotorespirometria, che si è dimostrata una valida alternativa per comprendere in modo più rapido l'impatto di tali fattori sull'attività fotosintetica della microalga. L'influenza di ciascun fattore sulla crescita di Chromochloris zofingiensis è stata studiata adottando l'approccio One-Factor-At-a-Time (OFAT) e il modello di crescita finale è stato ottenuto combinando il contributo individuale di ciascun fattore sulla velocità di crescita complessiva della *Chromochloris zofingiensis*. Le condizioni ottimali determinate in laboratorio dovranno essere applicate al reattore da 200L al fine di valutare la possibilità di adottare il modello anche a scala industriale. Durante questo studio, sono stati condotti i primi due esperimenti batch sul reattore tubolare, i quali hanno evidenziato una velocità di crescita significativamente inferiore rispetto a quella ottenuta nelle colonne a bolle.

Ciò potrebbe essere attribuito a diversi fattori, tra cui la diversa geometria e turbolenza a cui le cellule algali sono soggette, e l'elevata concentrazione di ossigeno disciolto (DOC) che tende a verificarsi nei reattori tubolari. A tal proposito, sono stati condotti ulteriori esperimenti fotorespirometrici per valutare come la crescita del *C. zofingiensis* diminuisca per elevati valori di DOC e le conseguenze di un eventuale accumulo una volta raggiunte le condizioni di saturazione. In conclusione, dai risultati ottenuti si consiglia in futuri studi sul reattore, di monitorare la concentrazione di ossigeno disciolto per assicurarsi che non raggiunga le condizioni di saturazione (raggiunte a circa 12 mgO_2/L) e preferibilmente rimanga al di sotto di 9 mgO_2/L, al fine di evitare una significativa diminuzione della crescita. Nel caso in cui i valori di DOC superino tali limiti, occorrerà adottare misure per migliorare l'efficienza del trasferimento di massa gas-liquido. Inoltre, per ottimizzare ulteriormente la crescita quando si opera a luce continua, si suggerisce di impiegare il modello di distribuzione della luce ottenuto in questo studio per aumentare l'intensità di luce incidente durante l'operazione e mantenere costante la luce media nel mezzo di coltura all'aumentare della concentrazione di biomassa. Per determinare il valore ottimale di luce media da mantenere costante, sarà necessario condurre ulteriori esperimenti batch sul reattore in diverse condizioni di illuminazione, seguendo l'approccio utilizzato in questo studio per le colonne a bolle. Ciò consentirà di individuare l'intensità luminosa media che massimizza la crescita e verificare se corrisponde a quanto riscontrato in scala di laboratorio in questo lavoro di tesi, o se la diversa geometria e dimensione del reattore comporta implicazioni sull'andamento della crescita in relazione alla luce.

Contents

Introduction

Chromochloris zofingiensis is a unicellular green alga that has gained considerable attention for its unique attributes and versatile applications, particularly in producing the powerful antioxidant astaxanthin. However, its industrial application is hindered by contamination issues, high energy requirements, and scalability challenges. Mathematical modeling plays a crucial role in predicting and optimizing microalgae growth, essential for assessing large-scale cultivation's profitability and sustainability. This thesis investigates the impact of key factors on *C. zofingiensis* growth and explores the implications of scaling up, aiming to develop an accurate mathematical model for predicting and optimizing its productivity. The thesis comprises four chapters.

- The first chapter provides an overview of microalgae, with a specific focus on the *C. zofingiensis* species. Key characteristics, applications, and the challenges associated with industrial cultivation are discussed. Additionally, the chapter analyses different factors that affect microalgae growth and presents the current state of the art regarding the development of mathematical models to predict their growth.

- The second chapter is dedicated to describing the cultivation systems used and the experimental protocols implemented during the study.

- The third chapter focuses on studying light attenuation in microalgal suspensions. The distribution of light intensity in tubular reactors under various light conditions and biomass concentrations will be assessed. Furthermore, a mathematical model capable of describing the obtained light profiles will be identified.

- In the fourth chapter, the effects of light intensity, temperature, nitrate, and phosphate concentration on *C. zofingiensis* growth are investigated. Mathematical models that predict the influence of these factors on microalgae growth are analysed.

- The fifth chapter examines the impact of high dissolved oxygen concentrations on the photosynthetic efficiency of *C. zofingiensis* by means of photorespirometry.

- Some final remarks and future perspectives conclude the work.

Chapter 1

Background

1.1 Microalgae characteristics and growth

Microalgae are unicellular photosynthetic microorganisms whose potential has been highlighted in the last decades due to the wide variety of applications in which they can be involved. There exist several hundred thousand species of microalgae in nature, out of which only a handful of them have been economically exploited (Chandra et al., 2019). They can differ significantly in size (from a few micrometres, to a few hundred micrometres) and can have a wide range of morphological variation (round, oval, cylindrical, and fusiform cells) as well as projections (thorns, cilia, etc.). The microalgal species can be distinguished by the light harvesting pigments present in the cell and can be classified in four main types (Metting, 1996): diatoms (Bacillariophyceae), green algae (Chlorophyceae), blue-green algae (Cyanophyceae) and golden algae (Chrysophyceae).

Microalgae growth in batch culture can be generally characterized by four phases (Béchet et al., 2013):

- The lag phase: the growth is delayed due to physiological adjustments in new environments.
- The exponential phase: the growth rate is constant and microorganisms grow at maximum speed; the number of microalgae doubles at regular time intervals.
- The saturation phase: the growth rate is zero. Light intensity reaches a saturation threshold, photosynthesis cannot process more photons and nutrients in the culture medium are exhausted.
- The death phase: the number of viable cells decreases with the stop of division and metabolic phase. It can occur if light intensity further increases beyond an inhibitory threshold, photosynthesis rate starts decreasing due to several factors such as depletion of nutrients, excess biomass concentration, overheating, pH disturbance, or contamination.

1.1.1 Application and advantages of microalgae

Considerable interest has been drawn towards the potential of microalgae for industrial exploitation over the past 70 years (Figure 1.1). Microalgae could be a viable solution for wastewater treatment since they assimilate phosphate and nitrogen, the main contributors to the eutrophication phenomena (Salama et al., 2017). Furthermore, they have a high carbon dioxide fixation rate, which can be used in flue gas treatment to reduce the concentration of this greenhouse gas in the atmosphere (Kumar et al., 2010).

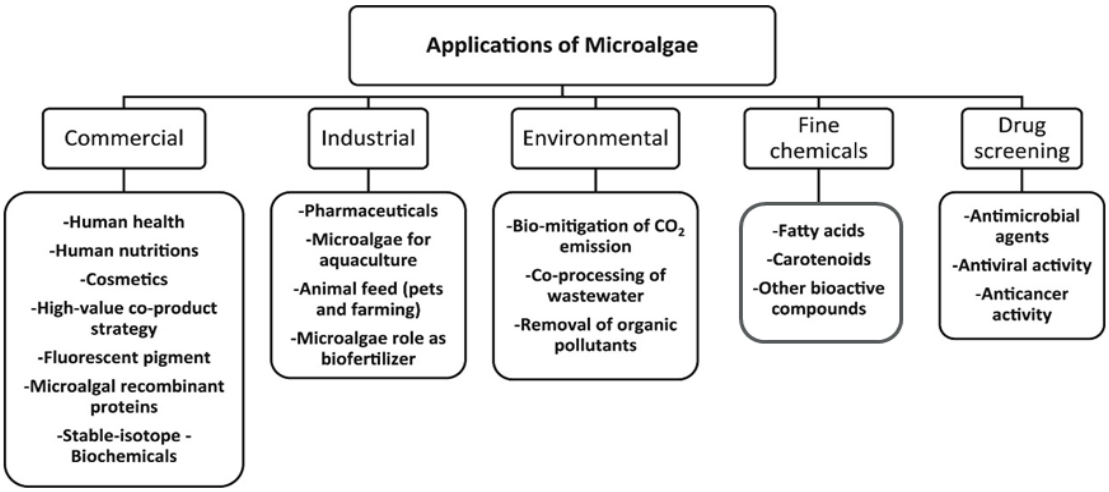

Figure 1.1 *Applications of microalgae in different fields (Rizwan et al., 2018).*

Another key attribute of microalgae is their capacity to produce long chain polyunsaturated fatty acids with positive effects on human health, they can also be a source of pigments and antioxidants for food, cosmetic and pharmaceutical industries (Vieira et al., 2020). Moreover, some species have gained significant interest in biofuel production thanks to their capability to store large amounts of triacylglycerol that can be then converted into biodiesel (Neofotis et al., 2016). The advantages compared to other crops are their high photosynthetic efficiency per area, and the possibility of cultivating them even in non-arable land avoiding the impact on agricultural land (Mata et al., 2010).

1.1.2 Factors affecting the photosynthetic process

Microalgae growth can be affected by several factors that can be divided in three categories (Mohsenpour et al., 2021):

- Abiotic factors including light, temperature, nutrients (CO_2, N, P, K, etc.), O_2, pH, salinity and toxins.
- Biotic factors such as bacteria, fungi, viruses, and other species in competition with microalgae.
- Operational factors including mixing and stirring conditions, dilution ratio, vessel geometry, and harvest frequency.

In the last century, extensive studies were conducted to explore the effects of these different factors on the growth and composition of algal cultures, contributing to a comprehensive understanding of their intricate relationships and potential applications.

1.1.2.1 Nutrients

The availability of nutrients, especially carbon (C), nitrogen (N) and phosphorus (P) can significantly affect the biochemical composition of microalgae and their growth kinetics. Due to the diversity of species, it is not possible to define a general molecular formula however the minimum nutritional requirements needed for their growth can be estimated by the approximate molecular formula $CO_{0.48}H_{1.83}N_{0.11}P_{0.01}$ (Christy et al., 2007). According to this formula, about 50% of biomass is composed of carbon, therefore high concentrations of carbon sources are required and depending on how this demand is met, microalgae can be cultivated at different conditions. In photoautotrophic conditions, microalgae rely on photosynthesis as their primary source of energy, they use light and carbon dioxide (CO_2) to produce organic compounds. In heterotrophic conditions instead, microalgae obtain their energy and carbon from external organic sources such as glucose, glycerol or cellulose hydrolysis products. Finally, mixotrophic conditions represent a combination of both photoautotrophic and heterotrophic modes of growth (Kim et al., 2013). The most important element after carbon is nitrogen, which is responsible for the production of proteins, vitamins, nucleic acids, and photosynthetic pigments (Chowdury et al., 2020). The most common nitrogen sources are nitrate, nitrite, urea and ammonium; nevertheless, nitrate is preferred for microalgae culture over ammonium salts due

to its greater stability and lower likelihood of causing pH shifts. Nitrogen can affect the biomass productivity and the cellular composition. Zhu et al. (2014) reported that under nitrogen starvation conditions, *Chromochloris zofingiensis* showed growth inhibition and increased lipid production. According to Feng. et al. (2012) the lipid content of *C. zofingiensis* was 65.1% in medium deficient of nitrogen, while only 33.5% was obtained from cells grown in full medium. Nitrogen limitation can result in a decrease in the cellular content of the thylakoid membrane, activation of acyl hydrolase, and stimulation of phospholipid hydrolysis, increasing the intracellular fatty acyl-CoA content (Chu et al., 2013). Phosphorus is another essential compound that has a significant impact on biomass productivity, lipid production, fatty acid yield and many cellular metabolic activities such as energy transfer, synthesis of nucleic acids, deoxyribonucleic acid (DNA), ribonucleic acid (RNA) and ATP (Atiku et al., 2016). Microalgae can absorb phosphorus in the form of polyphosphate or orthophosphate; however, it plays a less dominant role than carbon and nitrogen in the cellular duplication and the accumulation of lipids. Working at different concentrations of nitrogen and phosphorus can be an effective strategy to enhance the content of target substances; the N:P ratio in the culture medium plays an important role as shown by Yaakob et al. (2021) which summarizes the effect of nitrogen and phosphorus availability and starvation in different species of algae.

1.1.2.2 Light and Temperature

Light availability is the most important factor in the growth and productivity of photosynthetic microorganisms. Therefore, maintaining the light intensity within the optimal range is crucial to maximize microalgae growth. Below this range, growth is limited due to photolimitation, while exceeding this range leads to saturated conditions, resulting in an inefficient use of energy. Moreover, excessively high light intensity beyond the optimal range can induce photoinhibition and damage the photosynthetic apparatus (Wágner et al., 2018). Another important phenomenon to consider when working with a turbid media like algae culture is light attenuation: the irradiance inside microalgae cultures is not homogeneous but is a function of light intensity, culture depth, and biomass concentration (Chowdury et al., 2020). Light attenuation is affected by the absorption capacity of photosynthetic pigments, the self-shading effect by cells and light scattering caused by reactor wall and cells. To solve this problem, the concept of average irradiance has been introduced and will be discussed in §3.1. In addition to light intensity, the light wavelength has significant impact in microalgae growth and pigment

synthesis. The availability of specific wavelengths can influence the synthesis and composition of pigments in microalgae (Metsoviti et al., 2020). Depending on the types of pigments they contain, microalgae can absorb different wavelengths of light, mainly within the visible spectrum (PAR). Therefore, to maximize photosynthetic efficiency, it is essential to provide algae with light radiation that falls within the specific range absorbed by their pigments such as chlorophylls, carotenoids, phycoerythrin and phycocyanin. The two major groups of photosynthetic pigments in green algae are chlorophylls (green) and carotenoids (red-yellow). Chlorophylls absorb light in the blue (450–475 nm) and red (630–675 nm) spectrum bands, while carotenoids absorb light in the 400–550 nm spectral range. Chlorophylls are the main photon-harvesting pigments, while carotenoids serve as protective pigments, improving light absorption and utilization and providing defence against high irradiance and reactive oxygen species (Wagner et al., 2018). After nutrients and light, temperature plays the most important role in microalgae growth. The optimal temperature providing maximum growth rates is generally stated between 20 and 30 °C, although some thermophilic strains can endure up to 40˚C (Ras et al., 2013).

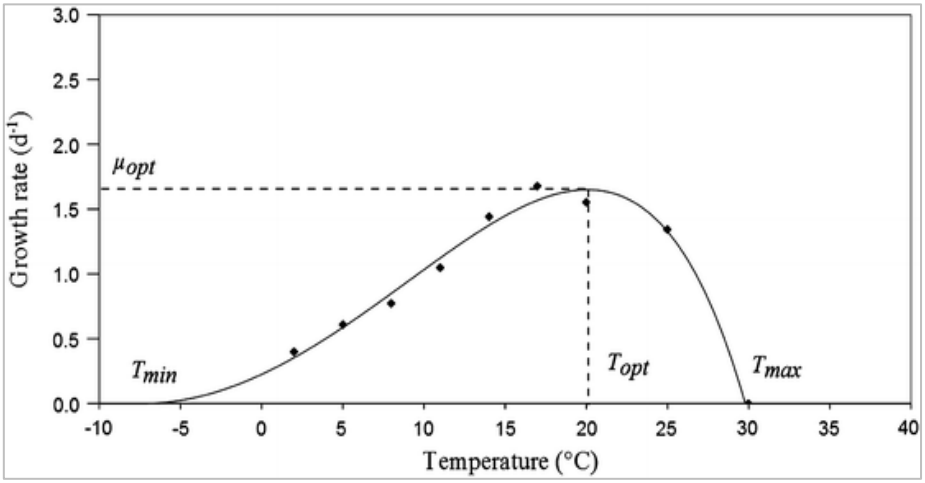

Figure 1.2. *Thermal growth curve of the microalgae species Astrionella formosa (Bernard and Rémond, 2012).*

Below the optimal temperature, an increase in temperature results in an enhancement of enzymatic activities related to the Calvin cycle which entail a positive effect on photosynthesis and cell division. Above the optimal temperature, the growth rate of microalgae decreases dramatically (Figure 1.2), and this is generally explained by heat stress, which can affect enzyme functionalities (inactivation, denaturation) or modify proteins involved in photosynthetic processes, thus inhibiting growth (Manhaeghe et al., 2019).

1.1.2.3 Dissolved oxygen

The dissolved oxygen concentrations (DOC) measured within the cultivation system is another crucial factor that can significantly affect microalgal growth. At high concentration, oxygen can compete with carbon dioxide for RuBisCo, which is the key enzyme in the Calvin cycle (Sforza et al., 2020). This phenomenon leads to the production of glycolate instead of the expected glyceraldehyde 3-phosphate at the output of the Calvin cycle. In addition, under high light conditions, the increased oxygen production along with the fluxes of photons and of electrons generated in Photosystem II significantly enhances the formation of reactive oxygen species (ROS). ROS can cause organelle dysfunction alteration of cell structures, and damage to proteins and membranes. High ROS concentrations induce oxidative stress, leading to cell mortality (López Muñoz et al., 2021). Photo-respirometric tests have shown that when the DO concentration is maintained below saturation levels, the photosynthetic oxygen production rate (OPR) of microalgae remains largely unaffected (Kliphuis et al., 2011). If the DOC exceeds this level, it becomes necessary to consider its impact when developing a mathematical model to optimize the production process and better control the growth conditions to avoid critical regimes where productivity decreases.

1.2 Microalgae commercial cultivation techniques

At the industrial level, a wide range of cultivation systems have been studied and developed for microalgae mass production. These reactors vary significantly depending on several factors such as the light source applied, the process mode (batch, semi-batch, continuous) and the reactor geometry (Ahmad et al., 2021). Basically, these systems can be categorized into two main types based on the cultivation method. The first one is conducted in open systems while the second cultivation method is conducted in closed, transparent systems. Open ponds are the most widely used at commercial scale as they have lower capital and operating costs. However, biomass productivity is lower than that achieved in closed systems, due to the dependence on the local weather and higher likelihood of contamination by other microorganisms. On the other hand, closed systems are becoming very popular and attractive due to the better control and higher production rates they offer; however, because of their high investment costs and energy requirement (particularly for mixing and cooling processes) their use is still limited. They can be defined as closed vessels for the photoautotrophic cultivation of microalgae in which energy is provided by artificial light or sunlight. They are characterized by many different geometric

configurations including vertical PBRs, flat plate PBRs, helical PBRs, tubular PBRs and internally-illuminated PBRs (Placzek et al., 2017). Vertical PBRs consist of vertical oriented tubes with a gas sparger at the bottom to facilitate mixing and gas mass transfer (Figure 1.3) and can be classified into bubble column PBRs and air lift PBRs. Vertical PBRs present numerous advantages such as high efficiency of photosynthesis, high potential of scalability, reduced risk of photoinhibition and photooxidation, cost-effectiveness and easy maintenance. Nevertheless, an inherent limitation of vertical PBRs is the small surface area available for light exposure, that is additionally reduced with the increase of column diameters. Flat panel systems are characterized by rectangular or square panels with shallow depths, typically made of transparent or translucent material. Agitation is provided by air bubbling or mechanical rotation of a motor through a perforated tube. Noteworthy advantages of flat panels include a high surface-to-volume ratio, uniform light distribution across the entire cultivation volume, and small concentration of dissolved oxygen. However, possible drawbacks are the risk of fouling and that scaling up requires the use of multiple modules and support structures (Ahmad et al., 2021). Tubular photobioreactors are manufactured using plastic or glass straight tubes, that are arrayed in vertical, inclined, helical, or serpentine configurations. The basic design principle of tubular PBRs can be divided into two parts. The first part is the tubular part or the reactor in which the microalgae are grown while the second one is the degasser unit which is used to remove the gas and the pump system which provides circulation and mixing of the microalgae culture. The serpentine tubular photobioreactor, as the one used in this work, consists of straight tubes connected by U-bends to form a flat loop (the photostage) that may be arranged either vertically or horizontally (Zittelli et al. 2013). These reactors are characterized by relatively low capital cost and very large illumination surface area that makes them suitable for both indoor and outdoor cultivation. On the other hand, some drawbacks could be the risk of biofilm accumulation on tube walls, the poor mass transfer and the possible fluctuations in pH, concentration of dissolved O_2 and CO_2 along the tube length (photoinhibition risk). To further delve into details, the recent review by Chanquia et al. (2022) analyses the current challenges and advantages of each different type of photobioreactors, from the more conventional ones widely used in the industry to the more innovative designs currently limited to laboratory-scale operations. Despite advancements in bioengineering and biotechnology to enhance algal growth efficiency in photobioreactors, open systems remain the dominant approach for industrial-scale algae cultivation. This is primarily due to unresolved technical challenges and the high investment and production costs associated with photobioreactors. Extensive research is

currently underway to address and resolve these challenges, by combining a wide variety of photobioreactor (PBR) types with innovative technologies and advanced methods of lighting, aeration, and mixing, along with a deeper understanding of the growth mechanisms under different conditions, new and efficient strategies for large-scale microalgae cultivation are expected to emerge.

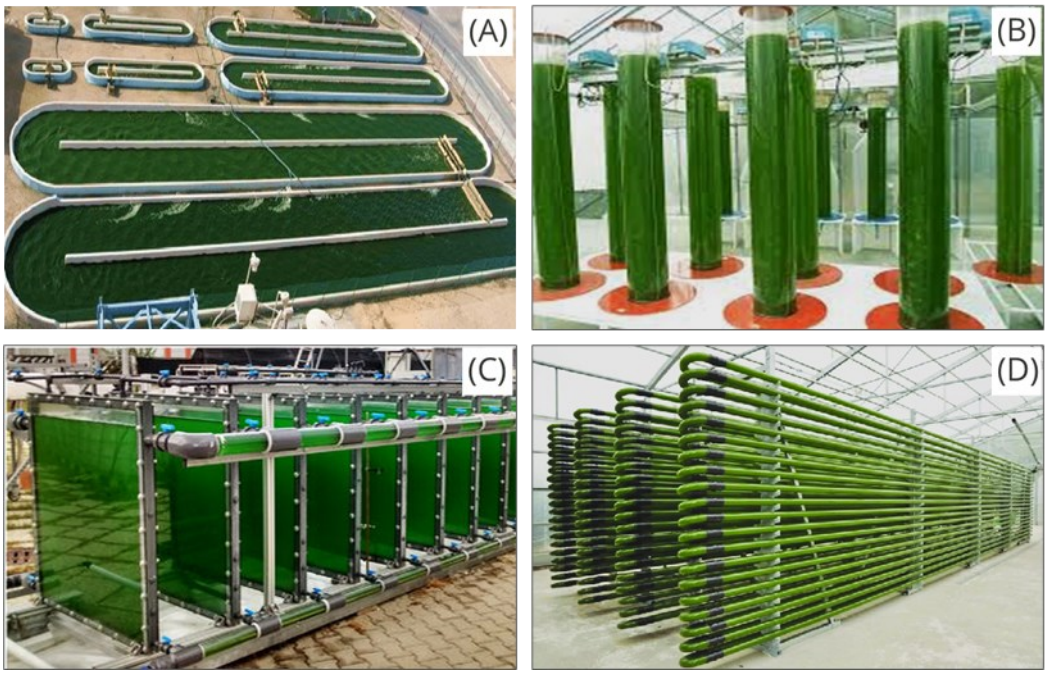

Figure 1.3. *Commercial-scale systems for microalgae production. (A) open ponds (Kumar et al., 2014); (B) bubble columns (J. Algal Biomass Utln.); (C) flat-plate reactor (Lindblad et al., 2019); (D) tubular reactor (Alaswad et al., 2015).*

1.2.1 Scale-up issues

In biotechnological processes, scale-up criteria are usually based on determining the relationship between the culture parameters and fluid patterns within the PBRs, which, of course, do not scale linearly with the PBR size. For example, while mixing culture in laboratory-scale PBR may be able to ensure that cells move along the light gradient within the same time scale as some biochemical processes, this is not the case for large scale PBRs. Therefore, it seems conceivable that kinetic models obtained in small-scale PBRs may be very far from the reality of what occurs in larger scale PBRs, where longer mixing times are involved and culture homogeneity is difficult to achieve. When scaling up, mixing time is certainly a key parameter to consider, along with pipe diameter and length (Torzillo et al., 2015). The flow pattern within the tube lumen can be regarded as a plug flow with minimal backward and forward mixing. Therefore, considerable spatial gradients of O_2 and CO_2 along the axis may occur and can gain

importance with the increasing of the length of the tubes. Some studies have shown that long tubular photobioreactors are characterized by these high gradients along the tubes and that very high dissolved oxygen levels are easily reached (Molina et al., 2001; Benner et al., 2022) negatively affecting both growth and biomass protein content. Additionally, when a tubular photobioreactor is scaled up by increasing the diameter of tubes, the illumination surface to volume ratio would decrease and the cells located at the lower part of the tube will not receive the necessary amount of light for their growth (due to light shading effect), unless there is a good mixing system. Another factor that can compromise large scale microalgae cultures is contamination as demonstrated in many studies (Carney and Lane, 2014; Kamravamanesh et al., 2019) in which cultures grown in closed systems were usually affected by contaminants despite protection from the outside atmosphere. Wang et al. (2012) and Borowitzka et al. (2017) highlighted the role of water used to prepare the medium as a potential vehicle for contamination. Moreover, it has been observed that algal cultures become more vulnerable to infection and predation in poorly mixed systems or under stressed conditions, which, as previously mentioned, are necessary to increase the production of biosynthesized compounds such as lipids and carotenoids.

1.3 Chromochloris zofingiensis

Chromochloris zofingiensis is a freshwater green alga that has gained considerable attention due to its unique attributes and versatile applications. It has a complicated taxonomy history. In fact, since Dönz isolated it (Dönz, 1934), it has been assigned to several distinct genus, including *Chlorella*, *Muriella*, and *Mychonastes*. Finally, after further observations Fučíková et al. (2012) reclassified *C. zofingiensis* into the genus *Chromochloris* within the class Chlorophyceae. It is characterized by a spherical shape, without flagellum, and with a cell diameter ranging from 2 to 15 μm. The life cycle of *C. zofingiensis* is simple and generally involves three phases: growth, ripening and division, which occurs through a consecutive pattern of multiple fissions as shown by Koren et al. (2021). Microscopic observation of *C. zofingiensis* cells under favorable (up) and stress (bottom) growth conditions. From the left to the right: transmission electron microscopy (CP, chloroplast; LD, lipid droplet; SG, starch granule); fluorescent microscopy (red indicates chlorophyll autofluorescence and green indicates neutral lipids); light microscopy.

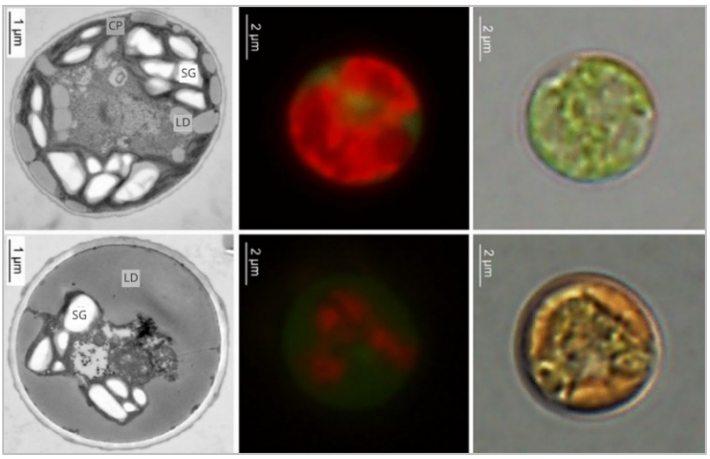

Figure 1.4. *Microscopic observation of C. zofingiensis cells under favorable (top) and stress (bottom) growth conditions. From left to right: transmission electron microscopy (CP, chloroplast; LD, lipid droplet; SG, starch granule); fluorescent microscopy (red indicates chlorophyll autofluorescence and green indicates neutral lipids); light microscopy, (Zhang et al., 2021).*

Under favourable growth conditions, the cells appear green while under stress conditions, reached through high light intensities and nitrogen starvation, the cells turn to orange (Figure 1.4). This color change is attributed to the synthesis of secondary carotenoids, including astaxanthin, a valuable antioxidant pigment with potential applications in the nutraceutical and pharmaceutical industries. Therefore, when carotenoid accumulation is to be achieved, nitrogen-deficiency conditions must be applied by providing a high carbon-to-nitrogen (C:N) ratio around 200:1 (Chen et al., 2017).

C. zofingiensis is recognized for its ability to produce high levels of lipids, particularly triacylglycerols (TAGs), but also proteins, essential amino acids and carbohydrates including starch. As a result, a notable feature of *C. zofingiensis* is its potential to simultaneously produce astaxanthin and TAGs. This characteristic opens up the possibility of generating multiple products, which can potentially yield higher revenue than extracting a single astaxanthin-lipid product (Wood et al., 2022). The TAGs can be used for biodiesel production or consumed as nutraceuticals. In addition, the starch content can be harnessed as a bioethanol feedstock or for bioplastics. Although other components such as proteins and carbohydrates are less explored in this species, they hold potential as valuable by-products for applications such as animal feed, fertilizers, biostimulants, enzymes, and cosmetics. (Figure 1.5) shows the wide range of potential products that could be obtained from *C. zofingiensis*.

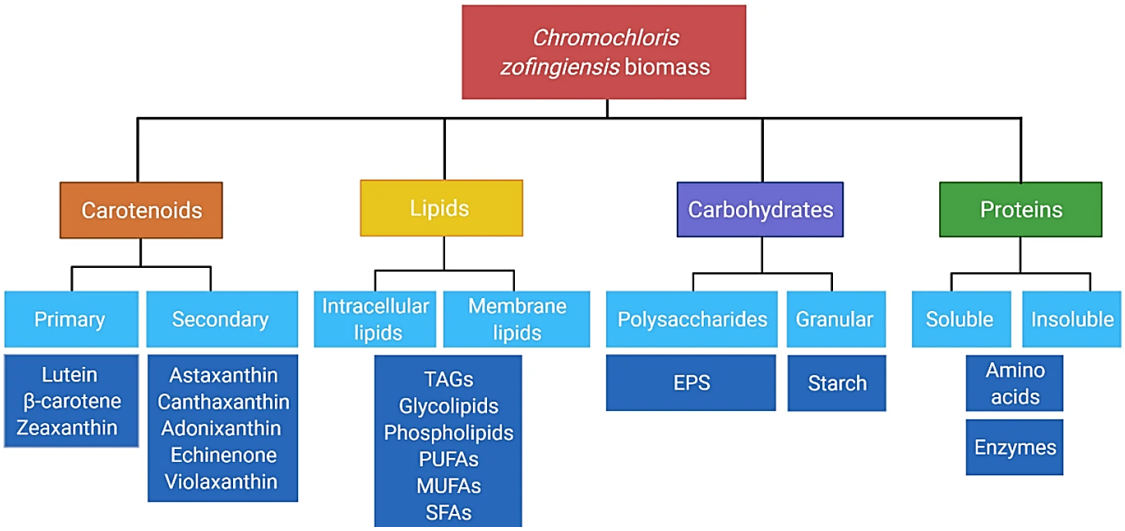

Figure 1.5. *Potential products from Chromochloris zofingiensis, (Wood et al., 2022).*

1.3.1 Astaxanthin

Astaxanthin is a red-orange oxycarotenoid pigment known for its strong antioxidant properties, which help protect cells from oxidative damage caused by free radicals. Astaxanthin has gained significant attention due to its potential pharmacological effects, including anticancer, antidiabetic, anti-inflammatory, immune-stimulating effects, as well as its favourable impact on skin, eye and cardiovascular health (Sztretye et al., 2019). It can be obtained synthetically from the petrochemical industry, or naturally through microorganisms such as *Chromochloris zofingiensis*, *Haematococcus pluvialis*, red yeast *Phaffia rhodozyma*, and the marine bacterium *Agrobacterium aurantiacum* (Fakhri et al., 2018). The microalgae *H. pluvialis* represents the major natural source of astaxanthin and the only one currently approved by the Food and Drug Administration (FDA) for human nutrition, while the other sources have only been approved for aquaculture. At the moment, the market for astaxanthin is predominantly dominated by synthetic production, accounting for 95% of the market share. This is primarily due to the prohibitively high production cost of naturally derived astaxanthin from *H. pluvialis*, which ranges from $2500 to $7000 per kilogram, in contrast to the comparatively lower cost of $1000 per kilogram for synthetic production (Wood et al., 2022). Nonetheless, natural astaxanthin is preferred due to its higher antioxidant activity and prevalence in the desirable esterified form compared to synthetic sources. Among other natural astaxanthin sources, microalgae are the

ones with the biggest potential in terms of productivity. *H. pluvialis* produces more astaxanthin on cellular basis than *C. zofingiensis*: the highest astaxanthin content for *C. zofingiensis* is 13.1 mg g^{-1} dry weight, still much lower compared to the 40 mg g^{-1} dry weight obtained with H. pluvialis (Sun et al., 2015; Zhang et al., 2021). However, *C. zofingiensis* could represent a promising alternative due to its ability to achieve higher growth rates and cell densities, and be less susceptible to contaminations (Wood et al., 2022). Despite the lower astaxanthin yield per cell, the potential reduction in production costs and time could propel *C. zofingiensis* into the high-value market of astaxanthin production. A detailed summary of research conducted on its production through *C. zofingiensis* under different culture conditions can be found in Zhang et al. (2021).

1.4 State of the art in mathematical modeling

The use of mathematical modeling plays a crucial role in predicting and optimizing the growth rate of microalgae, which is essential for assessing the profitability and sustainability of large-scale algae cultivation. The biomass concentration in a batch reactor assuming perfectly mixed conditions and without considering the cellular death could be described by the following mass balance equation (Koller et al., 2017):

$$\frac{dC_X}{dt} = \mu\, C_X \tag{1. 1}$$

Where C_x represents the biomass concentration [g L^{-1}], μ the biomass growth rate [h^{-1}] and t the generation time [h]. Solving Equation 1.1 involves determining the biomass growth rate μ, which is function of all the possible limitations that can occur in the cultivation system. Therefore, the selection of a specific growth kinetic model is a critical aspect of process modeling, as it must take into account the influences of all parameters. As a result, many different kinetic models have been reviewed by numerous studies, concerning the single and/or combined effects of the process conditions while keeping the other parameters at saturation levels. The following paragraphs summarize the main mathematical models developed to predict the biomass growth rate μ.

1.4.1 Light distribution model

The biomass growth rate is function of the light intensity and, as already mentioned above, the distribution of light in microalgae cultures is characterized by significant heterogeneity. Apprehending the spatial distribution of the light intensity inside the photobioreactor is a keystone for productivity optimization, therefore, it is necessary to define a rigorous treatment of radiative transfer inside the culture. As light penetration inside a turbid medium is affected by the incident polar angle of the radiation on the illuminated surface, it is necessary to consider the light source positioning with respect to the optical transparent surface of the reactor (Pruvost, 2019). Additionally, light distribution inside the reactor is mainly influenced by the light attenuation caused by the biomass, which brings to an exponential decrease of light intensity with depth. This phenomenon is due to the absorption of light by intracellular pigments and the light scattering by the particles and the resulting light gradient can be described by different models including the Lambert-Beer law, the two-flux model and the radiative transfer equation (RTE) which is far more complex and requires great computational costs (Ross et al., 2021). Considering the cultivation system under the one-dimensional hypothesis, the light attenuation occurs mainly along a single direction perpendicular to the illuminated surface, then simple radiative models can be applied with relative accuracy. The simplest one is represented by the Lambert–Beer law which can be defined by the following equation (Equation 1.2):

$$I = I_0 e^{-\xi z} \tag{1. 2}$$

Where I is the light intensity, I_0 is the light intensity entering the media perpendicular to surface, z is depth, and ξ is the attenuation rate which can be defined and calculated in different ways: It can be described as a linear function of biomass concentration as shown by Grima et al. (1994) or as function of chlorophyll concentration (Packer et al., 2011), while other research relates k to both chlorophyll as well as biomass concentration in the media (Darvehei et al., 2018). However, it should be noted that the effect of wavelength mentioned earlier, is not considered in any of these studies. Blanken et al. (2016) proposed a new formula (Equation 1.3) for light intensity inside the culture also considering this factor:

$$I(z) = \sum_{\lambda=400}^{700} I_\lambda(0) e^{a_x C_x z} \Delta\lambda \quad (1.3)$$

where $I_\lambda(0)$ is light intensity at the surface for wavelength λ, a_x is light absorption rate, C_x is biomass concentration, and z is depth of the point at which light intensity is calculated. To apply the Beer-Lambert Law, the culture medium must be isotropic, and light must not be scattered in the media, which is not correct when it comes to microalgal cultures. The aggregation of the effects of cell absorption and light scattering by cells into a single extinction coefficient has been stated to have poor accuracy with regard to modeling light attenuation in PBRs (Cornet et al., 1995). Therefore, some researchers proposed to overcome this issue and improve the model accuracy by developing modified versions of Equation 1.2 including an additional extinction coefficient that accounts for light scattering (Klok et al., 2013). A compromise between the complexity of the radiant transfer equation and the simplicity of the Lambert-Beer law was proposed by Cornet et al. (1995) and is known as the two-flux model. It was derived based on assumptions made by Schuster (1905), that takes into account absorption and scattering of light by cells and that provides an analytical solution. The two-flux approximation is expressed by Equations 1.4 – 1.6 below (Huang et al., 2015).

$$I = \frac{I_0 4\alpha}{(1+\alpha)^2 e^{\delta X z} - (1-\alpha)^2 e^{-\delta X z}} \quad (1.4)$$

$$\alpha = \sqrt{\frac{E_a}{E_a + E_s}} \quad (1.5)$$

$$\delta = \sqrt{E_a (E_a + E_s)} \quad (1.6)$$

where E_a is the mass absorption coefficient and E_s is the scattering coefficient. It should be noted that the two-flux approximation simplifies to the Beer–Lambert law if the effects of scattering can be ignored (E_s = 0), that is only at low biomass concentrations (Krujatz et al., 2015).

1.4.2 Growth kinetic model considering a light factor

Microalgae require a specific light level in order to reach the maximum growth rate, referred to as a saturated light level (Figure 1.6). As discussed above, if light intensity is far above the saturation level, the growth will be inhibited by light (called photoinhibition). On the other hand, if light intensity is below the saturation level, the growth will be limited by light (called light-limitation) (Darvehei et al., 2018).

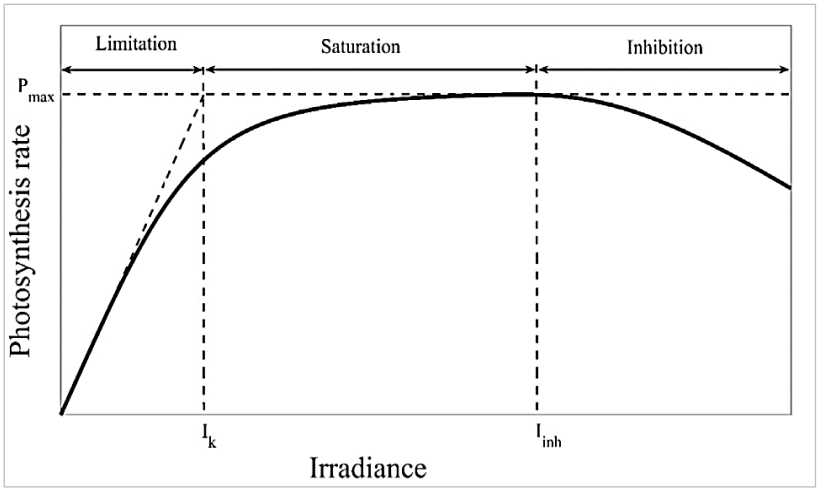

Figure 1.6. *A schematic of PI curve showing three light regions: (1) light limited, (2) light saturated, and (3) light inhibited (Darvehei et al., 2018)*

Many models have been suggested in the last few decades and according to Lee et al. (2015) they can be characterized into three different groups:

- First group: models consider light-limitation conditions and assume algae exist as individual cells. The models in this group have simple structures with two or three parameters so that they are easy to implement.
- Second group: models accounting for light attenuation by adopting an average light intensity or absorbed light intensity.
- Third group: models consider both light-limitation and photoinhibition.

A summary of the various proposed models can be found in Darvehei et al. (2018), here will be reviewed the details of the most prominent ones.
As part of the first group, the Tamiya model (Tamiya et al.,1953) is one of the earliest and most widely applied model that can be found in the literature and it is analogous to a Monod-type expression (Monod, 1949) in describing the effect of light on microalgae growth. In fact, the

equation is obtained by substituting the substrate concentration used in Monod, which considers only nutrient limitations conditions, with the irradiance:

$$\mu = \mu_{\max} \frac{I}{I + K_I} \tag{1. 7}$$

In this model the growth rate is related to the incident light intensity with two parameters: μ_{max} is the maximum specific growth rate and it indicates the maximum achievable specific growth rate when culture is in light saturated condition, K_I is the light half-saturation constant at which the specific growth rate is half its maximum value. If the incident light intensity I is lower than K_I, then the growth is limited by light according to first order kinetics; while when I is far above K_I, then the growth is independent from light and μ approaches to μ_{max}. Later, in addition to this model several empirical models have been developed. Van Oorschot (1955) considers an exponential equation known as Poisson function to describe the effect of light, while Bannister (1979) introduces a shape factor that enables the model to adjust its curvature based on the experimental data, and Chalker (1989) suggests hyperbolic tangent function to best fit the experimental data. The first group of models is preferable for low algae concentrations under laboratory conditions, assuming that there is minimal self-shading by the microalgae cells and so each individual cell equally receives incident light intensity. The models included in the second group instead, since light attenuation occurs, consider the light limitation associated with this phenomenon by adopting an average light intensity, which is determined by the incident light intensity, the light path, and the culture density. Grima et al. (1996) modified the Tamiya model by considering the light attenuation and by introducing an exponent in the formula, the parameter n describing the abruptness of the transition from weakly-illuminated to strongly-illuminated regions:

$$\mu = \mu_{\max} \frac{I_{av}^n}{I_k^n + I_{av}^n} \tag{1.8}$$

the Ogbonna model (1995) also includes the cell concentration X the volume of the reactor V and the non-illuminated volume fraction (*1-VF)* to take into account respectively the effect of cell concentrations and of dark on the light attenuation (Equation 1.9):

$$\mu = K\left\{\frac{I_{abs}}{XV} - I_{\max}(1 - V_F)\right\} \tag{1.9}$$

So far, all equations suggest that by increasing light intensity the growth rate increases in turn approaching its maximum value. Nevertheless, this is contradictory to what was previously said and shown in the diagram (Figure 1.6), where under a very high incident light intensity, a detrimental impact on cell growth is expected due to photoinhibition.

Therefore, Steele et al. (1962) pointed out that, in addition to the light limitation term, the photoinhibition term must be incorporated in the relation of light and growth by using an exponential expression (Equation 1.10):

$$\mu = \mu_{\max}\frac{I}{I_{opt}}e^{1-\frac{I}{I_{opt}}} \tag{1.10}$$

In this model I_{opt} represents the optimum light intensity to achieve the maximum growth rate after which any increase in light intensity results in lower growth rate.

Another equation later proposed by Aiba et al. (1982) added an inhibition term to Tamiya's equation:

$$\mu = \mu_{\max}\frac{I}{K_I + I + I^2/K_{i,L}} \tag{1.11}$$

Also other models in the same group involve an inhibition term in the denominator which is expressed as a function of the square of light intensity such as the Haldane model (Haldane et al., 1930), Talbot et al. (1991), Lee et al. (1987), and Bernard and Rémond (2012) in which different light intensities were considered: incident light intensity I in the Aiba model (Equation 1.11), average light intensity I_{av} in the Lee model, normalized incident light intensity I / I_{opt} in the Talbot model, and both I and I / I_{opt} in the Bernard and Rémond model.

Several models with more complex formulas have also been proposed, such as the modified Molina-Grima model (1994) and Muller-Feuga model (2003), which are commonly applied to estimate the growth rate of algae. The modified Grima model (Molina Grima et al., 1996) was proposed to improve the previous Grima model by modifying the parameters I_k and n in order to also account for the effect of photoinhibition.

On the other hand, in the Muller-Feuga model the growth rate is related to the average light intensity considering three parameters, including the maximum specific growth rate μ_{max}, the minimum light intensity for survival I_e and the optimum light intensity to achieve the maximum growth rate I_{opt}.

$$\mu = 2\,\mu_{max}\frac{(1-\frac{I_e}{I_{opt}})(\frac{I}{I_{opt}}-\frac{I_e}{I_{opt}})}{\left(1-\frac{I_e}{I_{opt}}\right)^2+\left(\frac{I}{I_{opt}}-\frac{I_e}{I_{opt}}\right)^2} \tag{1.12}$$

This model described the effect of light-limitation using $(I / I_{opt} - I_e / I_{opt})$ at the nominator and the effect of photoinhibition by using $(I / I_{opt} - I_e / I_{opt})^2$ at the denominator.

Some mechanistic models describing the interaction of cells with light have been available for several years, since Eilers and Peeters (1988) presented their pioneering work on the subject by assuming that the cells photosynthetic units (PSUs) can exist in three states: resting, active or inactive and depending on light intensity, their interaction changes.

Among other complex models, Camacho Rubio et al. (2003) developed a mechanistic model to account for photoadaptation, photoinhibition and the "flashing light effect". This model assumes that photosynthesis occurs in the photosynthetic unit (PSU, a minimum unit leading to the generation of NADPH and ATP), and the stored photochemical energy is consumed in an enzyme-mediated process that obeys Michaelis-Menten kinetics; in addition, this model uses a square-root dependence on irradiance to explain photoinhibition.

1.4.3 Growth kinetic model considering multiple factors

For Modeling the combined effects of different factors affecting microalgae growth two different approaches have been used:

- The model considers the dependency of different factors such as light, temperature, nutrients availability and dissolved oxygen as independent factors, so the relationship between them has been simplified to a multiplication of different functions representing each dependency.
- The model accounts for the interdependence of different factors coupling their effect in one single equation.

The first approach was adopted by Bernard and Rémond (2012) according to whom the growth can be expressed by the following equation:

$$\mu(T,I) = f(I)\ \phi(T) \tag{1.13}$$

where $\varphi(T)$ corresponds to the CTMI (the cardinal temperature model with inflexion) model (Equation 1.14) developed by Lobry et al. (1991):

$$\phi(T) = \frac{(T - T_{\max})(T - T_{\min})^2}{(T_{\text{opt}} - T_{\min})\left((T_{\text{opt}} - T_{\min})(T - T_{\text{opt}}) - (T_{\text{opt}} - T_{\max})(T_{\text{opt}} + T_{\min} - 2T)\right)} \tag{1.14}$$

It includes four parameters that have a direct biological interpretation, which makes the model rather straightforward to calibrate.

The dependency from light is instead described by the function $f(I)$, that is the reparametrized Haldane model suggested by Bernard and Rémond:

$$f(I) = \mu_{\max} \frac{I}{I + \frac{\mu_{\max}}{\alpha}\left(\frac{I}{I_{opt}} - 1\right)^2} \tag{1.15}$$

Where μ_{max} is the maximum growth rate at optimal light intensity I_{opt} and optimal temperature T_{opt} and α is the initial slope of the light response curve.

López Muñoz et al. (2021) proposed a new model to represent the combined effect of light, oxygen concentration and temperature (LOT-model) on microalgae growth. The LOT-model is obtained by coupling the Haldane model to represent the light impact and the Hinshelwood model (Hinshelwood, 1945) for the temperature effect and by introducing oxygen concentration in order to represent the oxidative stress affecting the cultures, adding a toxicity term in the expression of the net growth rate. Solimeno et al. (2015) developed a new mechanistic mathematical model that includes crucial physical and biokinetic processes for the description of microalgae growth in different types of cultures, particularly in wastewaters. The main relevant feature of the model, respect to any previous model for microalgae production, consists in the inclusion of a carbon limitation on the growth of microalgae, as well as a dynamic model for photosynthesis, photolimitation, light attenuation, and photorespiration. It is well-known, however, that the simultaneous effects of light and temperature on microalgal growth rates are interrelated and the hypothesis of uncoupling is incorrect especially at high light intensities,

since it is known that temperature plays a role in photoinhibition. The model developed by Dermoun et al. (1992) and the one suggested by Talbot et al. (1991) are some of the few models that account for the potential interdependence of light and temperature on the rate of photosynthesis. However, the tight coupling between light and temperature in these models can lead to problems of identifiability, partially due to the large number of parameters.

1.5 Aim of the thesis

Although microalgae cultivation in photobioreactors at the industrial level is still in its early stages of development, their immense potential is widely recognized. Consequently, numerous studies are currently being conducted to overcome the challenges associated with scaling up the process and enhance its efficiency. This work focuses on monitoring and modeling the specific microalgae species, *Chromochloris zofingiensis*, known for its exceptional potential in producing the powerful antioxidant, astaxanthin. The ultimate goal is to optimize the production of astaxanthin at large scale by implementing a three-step cultivation procedure: working under optimal conditions to maximize the growth, inducing stress conditions to enhance lipid and astaxanthin accumulation through nitrogen starvation, and subsequently supplementing with salt. To achieve this, the development of a predictive model that accounts for the effects of key factors on growth rate and biomass composition is crucial. Furthermore, it is essential to understand how scale-up and photobioreactor (PBR) geometry factors influence the model's response. This work is focused on the initial phase of the microalgal cultivation process and involves the monitoring of microalgal growth under optimal conditions, at laboratory-scale and in a 200L tubular reactor. The objective of this work is to conduct a comprehensive investigation into the effect of the main factors including light, temperature, nutrients concentration and dissolved oxygen, on the growth rate of microalgae. Understanding the influence of these different factors, along with the implications of scale-up, aims to contribute to the development of a mathematical model to accurately predict and optimize *C. zofingiensis* growth.

Chapter 2

Material and experimental methods

This chapter is dedicated to the presentation of instrumental tools, experimental procedures and analysis methods used for the thesis project. The experiments were conducted at the Institute of Natural Materials Technology at Technische Universität Dresden.

2.1 Culture medium and cultivation systems

The culture medium generally employed is the Bristol's Modified medium (BM), with the following composition: $NaNO_3$ – 7.5 10^{-1} [g/L], $MgSO_4 \cdot 7H_2O$ – 7.5 10^{-2} [g/L], $CaCl_2 \cdot 2H_2O$ – 2.5 10^{-2} [g/L], K_2HPO_4 – 7.5 10^{-2} [g/L], KH_2PO_4– 1.75 10^{-1} [g/L], NaCl – 2.5 10^{-2} [g/L], $ZnSO_4 \cdot 7H_2O$ – 2.87 10^{-4} [g/L], H_3BO_3 – 6.10 10^{-5} [g/L], $MnCl_2 \cdot 6H_2O$ – 1.69 10^{-4} [g/L], $CuSO_4 \cdot 5H_2O$ – 2.5 10^{-6} [g/L], $(NH_4)_6Mo_7O_{24} \cdot 7H_2O$ – 1.24 10^{-6} [g/L] and $FeCl_3 \cdot 6H_2O$ – 5 10^{-3} [g/L].

Due to cost constraints, it was not feasible to use the BM medium for the 200L reactor. In order to ensure consistency and facilitate comparisons across different cultivation systems, a custom fertilizer with the following composition was employed: 0.5 g L^{-1} of FertyII (N – 0.105 10^{-2} [mol/L], P – 0.5 10^{-3} [mol/L], K – 0.35 10^{-2} [mol/L], Mg – 0.6 10^{-3} [mol/L], Fe – 0.35 10^{-4} [mol/L]) and 0.5g/L of $NaNO_3$.

The fertilizer composition was determined through batch experiments conducted in the Cell-DEG system using HD10 cultivators. Different concentrations of FertyII and $NaNO_3$ were tested in order to identify the one that exhibited a similar growth trend to the BM medium and optimized the growth of the microalgae. The growth rate was monitored over a period of approximately 70 hours, with optical density measurements taken twice daily at 750 nm. The results of these experiments are presented in Figure 2.1.

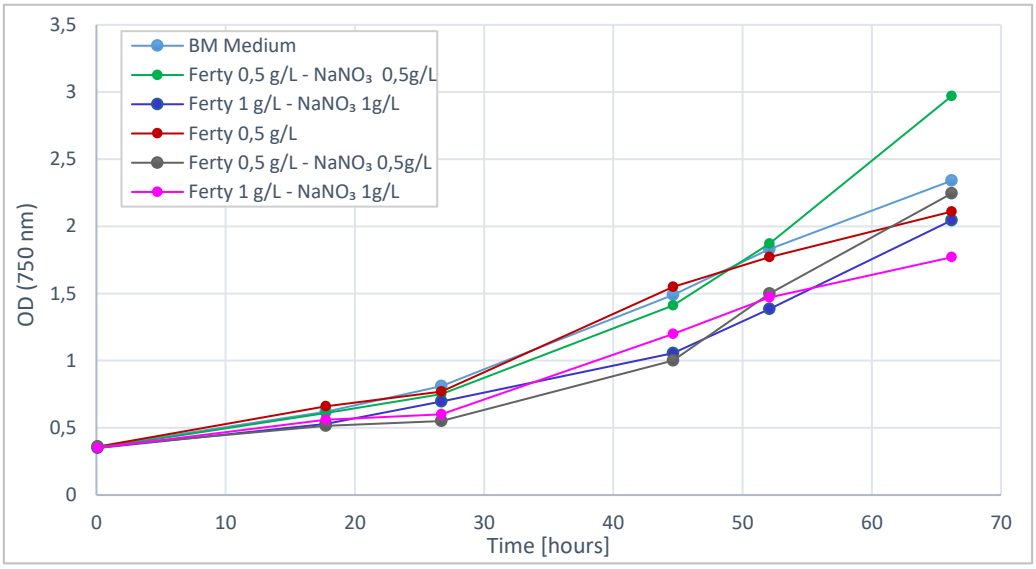

Figure 2.1. *Growth curves of C. zofingiensis at different concentrations of Ferty and $NaNO_3$.*

2.1.1 Bubble columns

Bubble columns are cylindrical vessels characterized by a very simple design with no internal partition and with the ratio of the height to the diameter always greater than 2 (usually in the range from 4–8, to ensure an optimum relation of the reactor's surface to its volume). The agitation of the suspension is realized by the presence of the gas phase, which is introduced into the culture in the form of small bubbles formed by a distributor located in the lower part of the column, which guarantees a sufficiently long duration of the contact between the algae and the gas phase. Many variants of sparger can be used such as rings, plates, nozzles, or evenly spread silica air diffusers which work like porous solids (Benner et al., 2022). The gas flow rate is usually controlled between 0.1 and 1 vvm (volumes of gas per volume of medium per minute). The air dispersed at the bottom can have an atmospheric composition or it can be enriched with carbon dioxide (Maroneze et al., 2016). Illumination in bubble column photobioreactors can be achieved through external or internal sources. Fluorescent tubes or LED lamps are commonly used to provide light. To ensure a more homogeneous distribution of light especially in case of large diameter, internal illumination methods have been explored, such as using light tubes parallel to the axis (Ding et al., 2021) or floating wireless light emitters suspended within the system (Heining et al., 2015). Incident light intensities usually applied with bubble column photobioreactors are between 15 and 220 µmol/ (m^2 s) (Hobuss et al., 2011). In this study the bubble columns will be illuminated through a LED panel placed in front of the column with a combination of blue and red light and the range of incident light intensity considered will be

between 30 and 150 μmol/ (m^2 s). Bubble column photobioreactors are typically made of transparent material if external illumination is applied, such as polyvinyl chloride, plexiglass or glass which is the only one that allows thermal sterilization (Benner et al., 2022). Temperature is controlled by transparent double jackets around the bubble column or by placing the bubble column in an incubator. Another possibility is to use stainless steel tubes as a heat exchanger inside the bubble column López-Rosales et al., 2016). These systems are commonly used in research, because they are characterized by low cost as they lack complexity of instrument parts and by great gas holdups providing a satisfactory heat and mass transfer (Kumar et al., 2011). In this study bubble columns will be used as pre-culture systems and for conducting experiments to investigate the effect of temperature, light intensity, and oxygen accumulation on *C. zofingiensis* growth. In Figure 2.2 is shown a typical 1 L bubble column used to monitor microalgae growth during batch experiments.

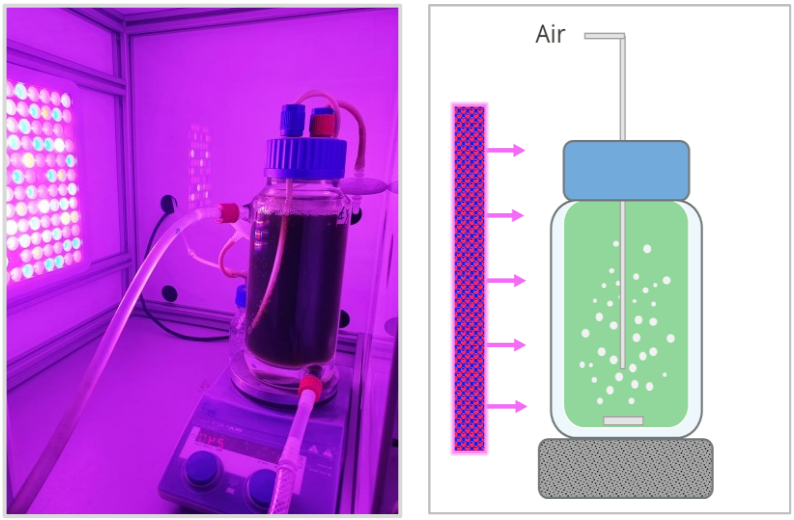

Figure 2.2. *Experimental set-up of batch experiments using bubble column.*

For the batch experiments, atmospheric air will be supplied to replicate the conditions applied in the 200 L reactor, while when it is used for the pre-inoculation (as for photorespirometry), the air supplied will be enriched with CO_2 to optimize the growth rate. Additionally, a magnetic stirrer will be employed to enhance the turbulence within the system.

2.1.2 Cell-DEG system

It is an innovative technology for photoautotrophic high-density cultures that consists on two-tier vessels over a shaken platform. The inferior vessel contains air enriched with CO_2 that can be regulated either through a carbonate buffer or controlled CO_2 injection, depending on the volume of the high-density cultivators (HDCs). The upper vessel contains the liquid culture and the turbulent gas phase, which is exchanged with the atmosphere by diffusion. The two chambers are separated by a thin highly gas-permeable membrane in polypropylene (Chanquia et al., 2022). The spatial separation of CO_2 supply from oxygen release effectively minimizes CO_2 loss to the atmosphere, which can be considered negligible compared to its consumption during photosynthesis. In all Cell-DEG HDCs turbulence is achieved using high-frequency orbital shakers, ensuring very low shearing stress on the cells. The turbulent liquid flow close to the membrane surface enables rapid bubble-free mass transfer of CO_2 into the culture, thereby preventing CO_2 deficiency even at high volumetric rates of carbon assimilation. Furthermore, the intermittent light regime with short mean durations of the light/dark cycles created by the turbulent mixing allows for a high quantum yield of photosynthesis, even under intense artificial lighting.

Figure 2.3 . *Experimental set-up of batch experiments using Cell-DEG HD100 cultivators.*

Overall, Cell-DEG HDCs offer a highly efficient and controlled environment for achieving photoautotrophic high-density cultures (Dienst et al., 2020). However, the total amount of biomass that is possible to obtain is limited, making their use primarly focused on the production of biomass at the research and preparative scale. In this study HD10 cultivators and HD100 cultivators (presented in Figure 2.3) will be used for different purposes: pre-cultivating

C. zofingiensis for the batch experiments, monitoring the growth rate at different nitrate and phosphate concentrations as well as identifying the best composition for the fertilizer to use in the experiments to replace the BM medium in the 200L reactor.

2.1.3 The 200L reactor

The 200L tubular reactor is mainly composed of two units: the solar loop in which biomass growth takes place and the degassing tank (Figure 2.4). The role of degasification tank is concerned with removal of O_2 produced during photosynthesis. The algal culture is circulated from the tank into the solar loop and returned into it, which prevents the photoinhibition phenomenon. The solar loop consists of slightly inclined, transparent tubes and bends with a diameter of 63 mm (inner diameter: 60 mm).

Figure 2.4. *The 200L tubular reactor during the first phase (on the right) and second phase (on the left) of the operation.*

The reactor is operated in a batch or semi-continuous mode. The circulation is achieved through an airlift using a gas flow rate of 20 L min^{-1}, whereby air is injected to the inlet of the solar loop by means of a compressor. Oxygen has to be removed from the suspension by introducing air to the liquid in the degassing tank. Thereby, gas insertion is supposed to occur when the outflow of the solar loop encounters the liquid surface in the degassing tank, resulting in mixing movements. The reactor is equipped with sensors to continuously measure turbidity, temperature, pH, dissolved oxygen concentration and light intensity value during operation with a time interval of 1 minute. LED lights are mounted on the upper side of the wall of each tube and can be adjusted in both intensity and colour (red, white, blue and white light) (Figure 2.5). In this study, a constant white light intensity was applied to monitor changes in biomass

concentration and average light intensity inside the reactor over time. Due to issues with sensor functionality the measurement of dissolved oxygen concentration will not be considered in this study. The linear relationship between the incident light intensity expressed as a percentage within the reactor and the light intensity expressed in μmol/(m^2 s) is depicted in Figure 2.6, while the relationship between turbidity and biomass concentration (g/L) is discussed in the next section § 2.2. Throughout the batch operation, it was assumed that both pH (approximately 8.7) and temperature remained constant, although slight fluctuations were observed within a maximum range of 1.5 °C. Since no heat exchange was employed, the temperature variation was influenced by the specific time of the year when the study was conducted, with temperatures around 20°C in January and approximately 25°C in March.

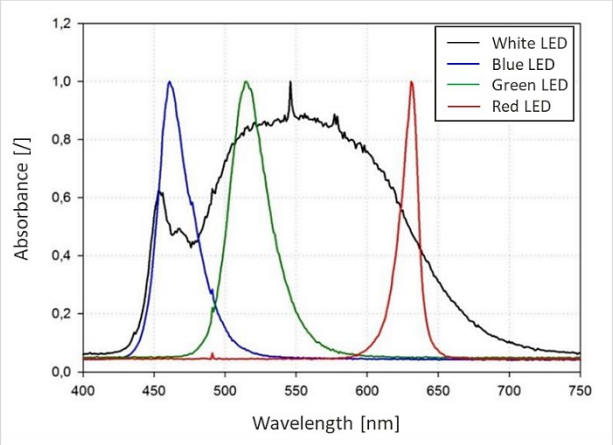

Figure 2.5. *Light emission spectrum of the LED-light sources of the 200L reactor*

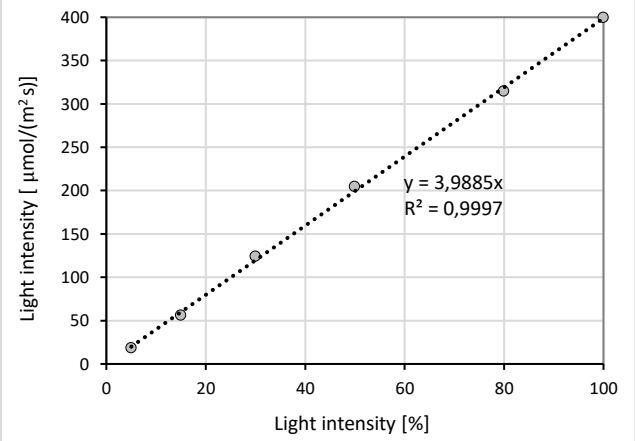

Figure 2.6. *Linear correlation for the incident light intensity of the 200L reactor.*

2.2 Experimental procedures

2.2.1 Dry weight measurements

In this study, the growth rate of *C. zofingiensis* will be monitored at laboratory scales by measuring the optical density, while for the 200L reactor, turbidity sensor will be used. To determine the biomass concentration in terms of g/L, it is essential to establish the relationship between these measurements. For this purpose, two different procedures, the filtration method and the freeze-drying method, have been employed to measure the biomass dry weight and evaluate the corresponding correlations. The filtration method involves washing a known

amount of culture (10 ml) with deionized water and performing vacuum filtration by the use of cellulose nitrate filters (0.2 µm porosity) previously dried at 60°C for 4 hours and weighed after drying (Figure 2.7).

Figure 2.7. *Experimental set-up of vacuum filtration.*

The filters are washed with deionized water both before and after adding biomass. After filtration, the filters (on which the microalgae are deposited) are placed in an oven at 60°C for 24 hours to remove any residual moisture. At the end of the drying process, the filters are weighed one more time in order to obtain the net weight. Dividing this value by the initial known volume, the dry weight (DW) of the culture is obtained.

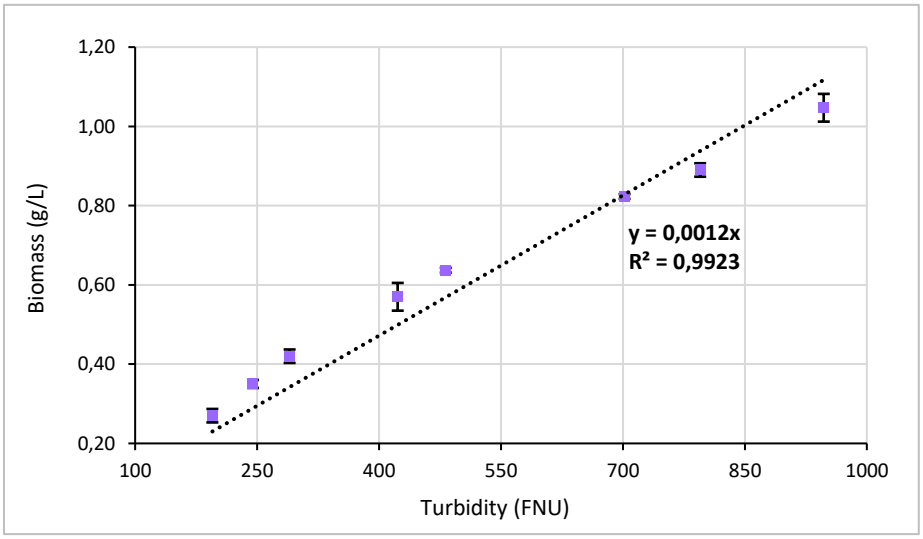

Figure 2.8. *Linear correlation between Biomass concentration and Turbidity determined using the vacuum-filtration method.*

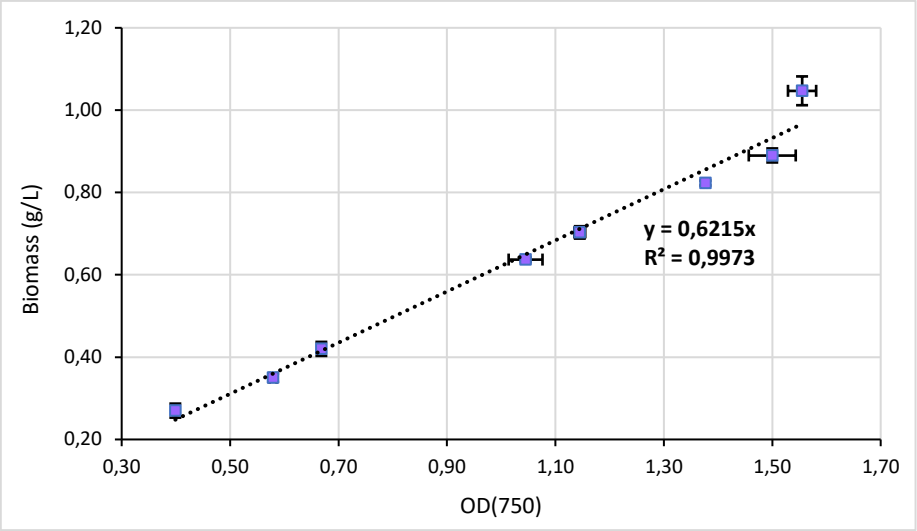

Figure 2.9. *Linear correlation between Biomass concentration and Optical density determined using the vacuum-filtration method.*

To increase the accuracy of the results, three replicates are analyzed for each sample. Figures 2.8 and 2.9 illustrate the turbidity and the optical density measured in the 200L reactor with the corresponding calculated dry weights and the linear correlations obtained.

The freeze-drying method is another approach used to measure the dry weight of microalgae biomass. In this procedure, a known volume of culture (50 mL) is first transferred into pre-weighed falcon tubes. The tubes are then centrifuged for 10 minutes at 15000 rpm to separate the supernatant from the pellet. The supernatant is carefully removed, and deionized water is added to the tubes that are centrifuged again to ensure thorough washing of the pellet. The tubes containing the pellet are stored at -80°C and then placed in a freeze-dryer, where the frozen culture is subjected to sublimation, through which the remaining water content is removed from the pellets. After the sublimation is complete, the tubes containing the dried biomass are weighed again to determine the net weight of the dry biomass. By dividing this weight by the initial known volume, the dry weight (DW) of the culture is calculated. Similarly to the filtration method, triplicates are typically analyzed for each sample to ensure the accuracy of the results. The freeze-drying technique offers the advantage of preserving the cellular structure and composition of the microalgae due to the gentle drying process. This is particularly beneficial when studying the biochemical properties or functionality of the microalgae biomass. Aljabri et al. (2023) in their work compare different drying techniques proving that the freeze-drying preserves the highest amounts of chlorophyll, proteins, and lipids but requires the highest amount of energy compared to the others methods. Figures 2.10 and 2.11 show the linear correlation obtained between dry weight, OD and turbidity, from the 200L reactor samples. The

results obtained through this second approach show consistency with the previous results.

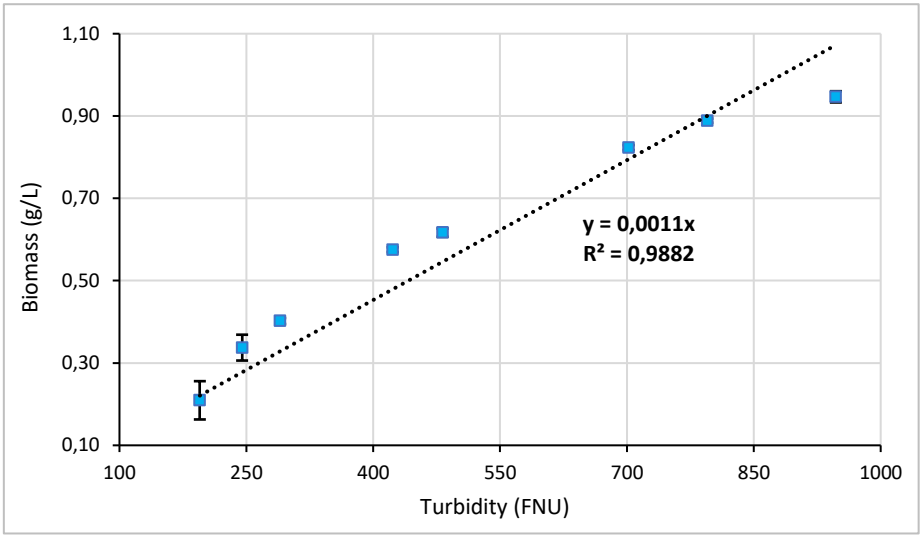

Figure 2.10. *Linear correlation between Biomass concentration and Turbidity determined using the freeze-drying method*

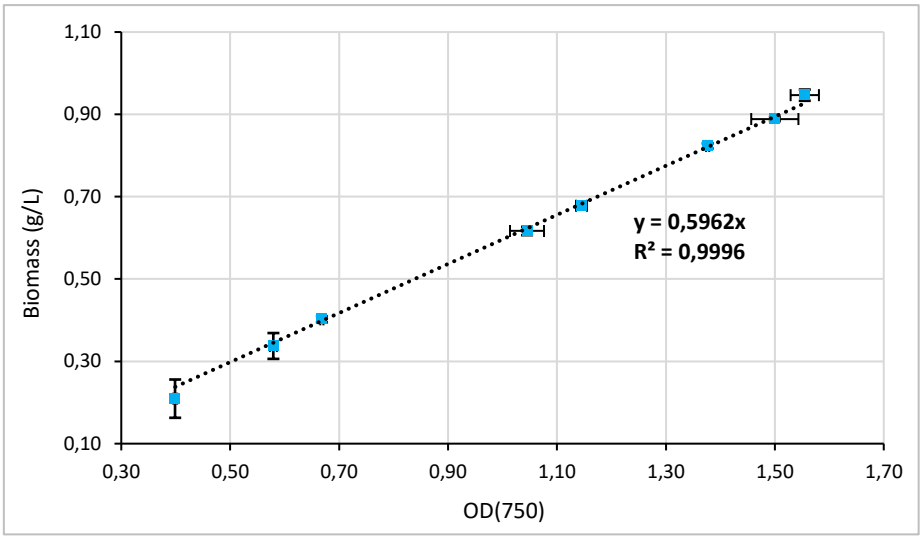

Figure 2.11. *Linear correlation between Biomass concentration and Optical density determined using the freeze-drying method.*

2.2.2 Photorespirometry

In recent years, photorespirometry has emerged as a simple and efficient method for studying the growth kinetics of microalgae. Since oxygen is obtained as a by-product of photosynthetic reactions, this technique takes advantage of the oxygen evolution rate over time to evaluate photosynthetic rates. Additionally, it allows for the quantification of the oxygen consumption associated with algal respiration. Indeed, the basal respiration that can be determined by

monitoring the oxygen consumption during the dark phase is represented by OPR_D, while the net oxygen production rate (OPR_L), which can be monitored when the algae are exposed to light, is determined by the combination of photosynthesis and respiration processes (Sforza et al., 2020). By analyzing these factors indication of the phototrophic growth can be obtained. The gross oxygen production rate (OPR_{GROSS}) representing the overall photosynthetic oxygen production can be assessed by calculating the difference between OPR_L and OPR_D as follows:

$$OPR_{GROSS} = OPR_L - OPR_D \tag{2.1}$$

In this equation, the subscripts L and D refer to light and dark conditions respectively, and OPR_D is obviously characterized by a negative value. Photorespirometry has been extensively used to investigate the effects of environmental parameters and estimate the optimal growth conditions for phototrophs. In suspensions of photoautotrophic microorganisms, it is essential to note that the changes in dissolved oxygen over time are influenced not only by the photosynthetic oxygen production rate (OPR) but also by the oxygen mass transfer from the liquid to the gas phase and it is described by Equation 2.2:

$$\frac{dC_{O_2}}{dt} = k_L\, a\, \left(C^*_{O_2} - C_{O_2}\right) + OPR \tag{2.2}$$

The term of the oxygen mass transfer is characterized by the oxygen mass transfer coefficient (k_La) and by the driving force represented by the concentration difference between the current DOC (CO_2) and the solubility concentration of oxygen in the liquid (CO_2*), which is determined by Henry's law:

$$C^*_{O_2} = H_{O_2}\ p_{O_2} \tag{2.3}$$

Where H_{O2} is the Henry constant which is dependent on temperature and p_{O2} is the oxygen partial pressure. The k_La can be determined by measuring the re-aeration rate of the medium after deoxygenation, typically achieved by stripping with nitrogen bubbling. However, according to Krujatz et al. (2020), which employed a similar methodology and experimental setup as this thesis for photorespirometric experiments, the k_La is several magnitudes lower than the photosynthetic OPR. Thus, in this study, the contribution of mass transfer has been assumed

negligible, and the following simplified equation will be considered:

$$\frac{dC_{O_2}}{dt} = OPR \tag{2.4}$$

Generally, photorespirometric experiments (Figure 2.12) involve batch tests consisting of alternating light-dark phases, which can be repeated over time to obtain replicated values and assess their statistical significance.

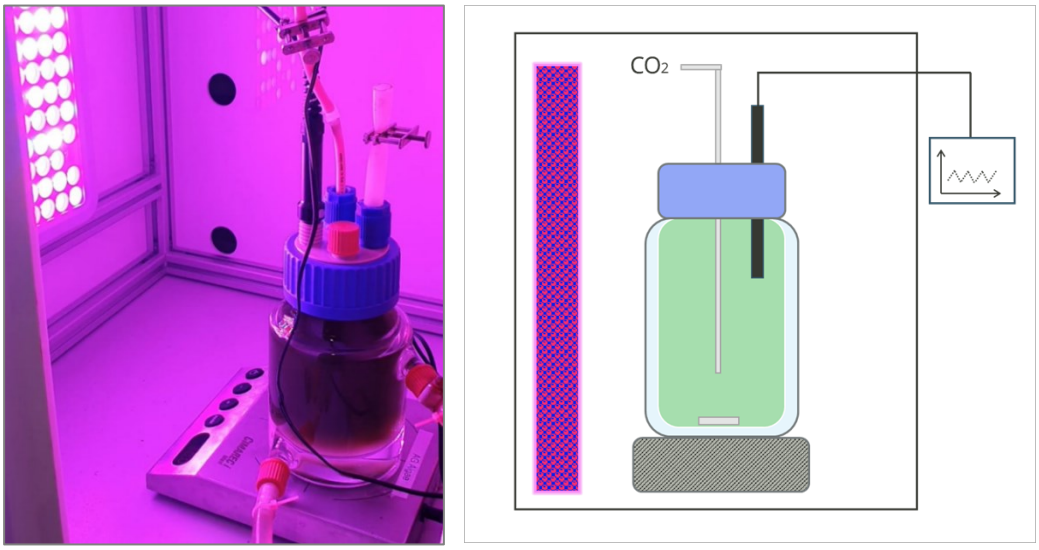

Figure 2.12. *Set-up of photorespyrometry experiment*

In some cases, batch experiments are also conducted under constant lighting conditions (i.e. only the light or the dark phase is considered during the test), however it is important to note that in such cases it is not possible to evaluate the gross oxygen production rate. Recently photorespirometric studies were focused on investigating the impact of light intensity and light spectrum, the availability of nutrients, the dissolved oxygen concentration and the main physical/chemical parameters (pH, temperature, salinity) on microalgae growth. In the present study, a similar respirometry protocol to that developed by Sforza et al. (2019) was applied to determine the impact of temperature, light intensity and high dissolved oxygen concentrations on the growth of *C. zofingiensis,* and to estimate the model kinetic parameters to describe this growth. The detailed protocol and experimental setup of the conducted respirometry experiments are explained in §4.2.

Chapter 3

Light intensity distribution

Light availability is one of the most important factors affecting microalgae growth. Therefore, the use of mathematical models that accurately reflect the dynamic of light distribution is critical to ensure effective reactor operation. This chapter provides a better understanding of light transmission during microalgal cultivation. The distribution of light intensity in tubular reactors under different biomass concentration and light conditions will be assessed, and a mathematical model able to describe the obtained light profiles will be identified.

3.1 Effect of biomass concentration

The experimental setup involved using a cylindrical tube, identical to the tubes used in the tubular reactor at PUEVIT company (PUEVIT GmbH, Dresden, Germany), as a measuring container. Light intensity was measured using two different devices. A light sensor capable of being immersed in liquid was used to measure the light intensity within the culture inside the tube. Additionally, a spectrometer was used to also detect the wavelength of the applied light.

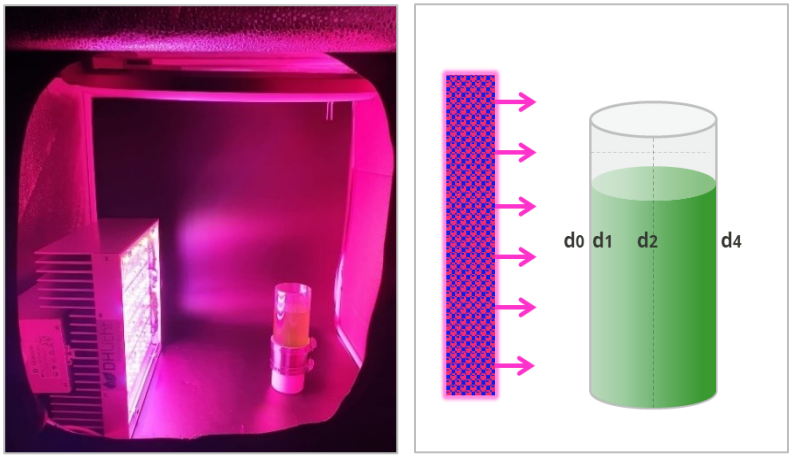

Figure 3.1. *Set-up of light attenuation measurements within Chromochloris zofingiensis culture.*

The tube was placed in a light-proof box and continuous artificial light was provided on one side of the tube by a LED panel whose colors and intensity were specially adjusted to reproduce the same light conditions used for the tubular reactors of the Puevit Company and for the 200L reactor of the P20 Lab. Therefore, in the first case a combination of blue and red light with an incident light intensity equal to 200 µmol/(m² s) was applied, while in the second case a white light with an incident light intensity equal to 220 µmol/(m² s) was used. The sensor was placed in four different positions: in front of the tube (*d*1), inside the tube near the wall (*d*2), in the middle of the tube (*d*4) and behind the tube (Figure 3.1). Taking into account the impact of the tube thickness, it was also possible to estimate the light intensity at the end of the tube on the inner side (*d*3). This was achieved by analyzing the difference in light intensity measured in the tube, when it is empty, between positions *d*1 and *d*2 and applying the obtained correlation to the measurement taken behind the tube. Measurements were conducted at various concentration values, starting with a concentrated solution with OD_{750nm} of 2. Subsequently, the solution was progressively diluted, and measurements were repeated until OD_{750nm} around 0.2 was attained.

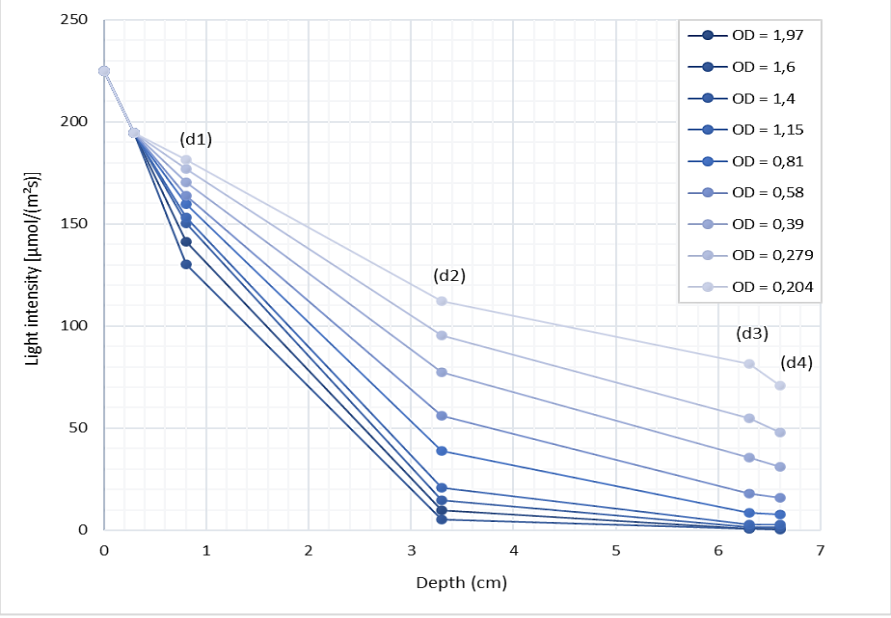

Figure 3.2. *Light intensity distribution within the tube at different OD considering the white light.*

Figure 3.2 represents light intensity values measured with white light and provides a graphical representation of how the light intensity through a *C. zofingiensis* culture changes along the tube as the concentration of cells in the microalgal suspension increases. Within a distance of less than 4cm, the light intensity has already decreased by approximately 40% for the lowest

biomass concentration under investigation. Towards the end of the tube, when the optical density is low (about 0.5), around 70% of the incident light is absorbed by the culture, and this absorption increases to 95% at an optical density of 1.

3.2 Effect of light wavelength

Light absorption characteristics of microalgae are also significantly influenced by the light spectrum. Figure 3.3 illustrates the variations in the light intensity measured within the tube when using two distinct light spectra, highlighting how differently light is absorbed. It is evident that the pigments primarily absorb blue and red light, excluding the dark red range (> 680 nm). This suggests that the absorption spectrum of chlorophylls encompasses wavelengths in the blue and orange-red light range.

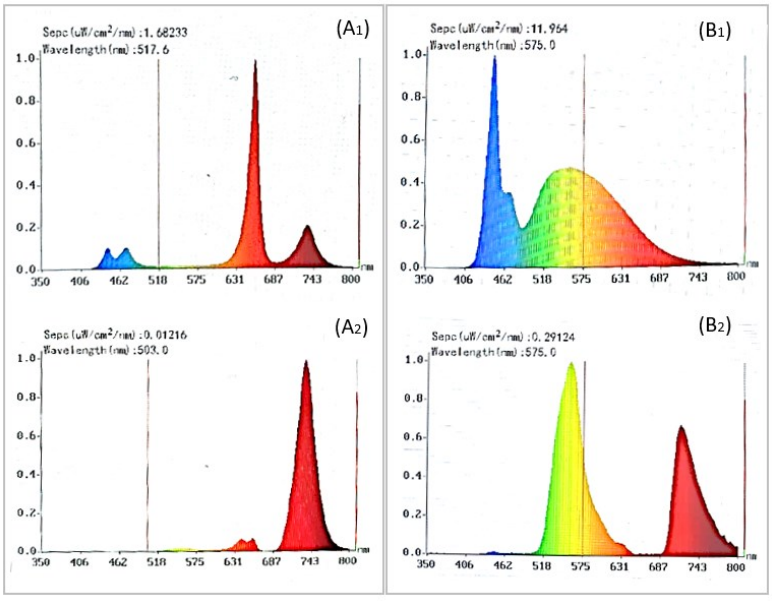

Figure 3.3. *Comparison of light spectra measured in an empty tube (top) and a tube filled with microalgal solution under blue-red light (A) and white light (B) conditions.*

Figure 3.4 shows the variations in light intensity, measured at the center of the tube (d2), as a function of optical density, for the two different light conditions applied. It is evident that the light distribution profile differs between white light and blue-red light. Notably, for the same biomass concentration, the light intensity measurements obtained with the blue-red light are significantly lower.

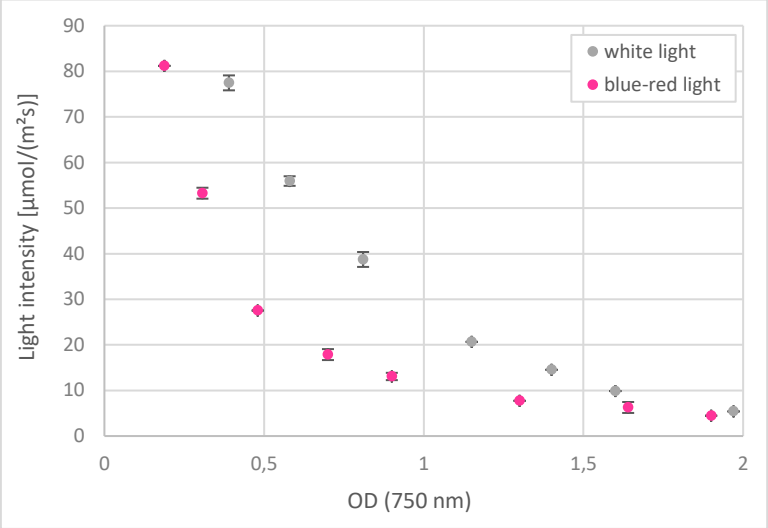

Figure 3.4. *Comparison of light intensity measured at the center of the tube at different optical densities (OD) under blue-red light and white light conditions.*

As biomass concentration increases, there is a more pronounced decrease in blue-red light intensity. At optical density of approximately 0.7, the light intensity with white light is around 40 µmol/(m² s), whereas with blue-red light it reduces to approximately 15 µmol/(m² s), indicating that nearly 95% of the intensity has been absorbed. This difference can be attributed to both the lower incident light intensity (100 µmol/(m² s) compared to 120 µmol/(m² s)) and the enhanced absorption of this wavelength by the pigments. These findings highlight the importance of considering not only the light intensity but also its wavelength when modeling light distribution. Since absorption of different wavelengths and microalgae pigmentation are closely interconnected, modifying the biomass composition, such as increasing the accumulation of astaxanthin, will inevitably affect light attenuation. Consequently, conventional light attenuation models that only account for biomass concentration (Beer–Lambert model, Cornet model, etc.) are no longer suitable for distinguishing the light distribution characteristics in microalgal suspensions with different pigment contents.

3.3 modeling light intensity

As discussed earlier in §1.4, different model complexities have been developed to account for light intensity in the PBRs. The simplest mathematical equation for predicting light distribution is the Lambert-Beer law (Equation 1.2). Knowing the incident light I_0, the depth z which corresponds to the inner diameter of the tube (6cm), and the values of light intensity measured

at that depth for each optical density, the only remaining unknown parameter is the extinction coefficient ξ which is function of the biomass concentration.

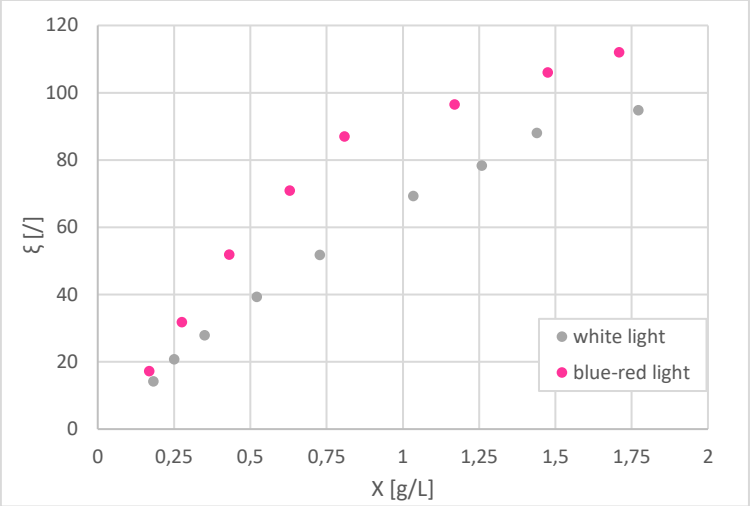

Figure 3.5. *Comparison of extinction coefficient measured at the center of the tube at different biomass concentration under blue-red light and white light conditions.*

The biomass concentration is estimated from the optical density through the linear correlation established by measuring the dry weights as described in §2.2. Figure 3.5 illustrates the relationship between the extinction coefficient ξ, evaluated through the Lambert-Beer law, and the biomass concentration, for the two different light conditions applied.

As mentioned above ξ can be expressed in different way. The simplest one is by defining it as the product of an absorption coefficient k and biomass concentration X in order to decouple the effect of biomass concentration on light attenuation:

$$\xi = k\,X \tag{3.1}$$

With this assumption a single parameter is used to describe light absorption disregarding the effects of light scattering. Since scattering cannot be neglected, especially in dense microalgal cultures, the equation may be useful as a first approximation to describe light regime in a photobioreactor, but a more comprehensive expression is required to obtain an accurate prediction of microalgal growth and minimize uncertainty in model predictions. Therefore, more complex expressions involving multiple empirical parameters have been proposed to better define the extinction coefficients. In this study the light distribution was modeled using

the Lambert Beer law (with ξ defined by the previous equation) and the Schuster's law (Equation 1.4). A comparison was made between the two models to assess the difference in results when accounting for the scattering effect. The different model structures were implemented in Python, and the parameters were estimated using the curve_fit function based on the Levenberg-Marquardt algorithm in order to minimize the sum of squared errors between the model function and the observed data. The estimated parameter values are presented in Table 3.1. The optimization of the model parameters based on the two sets of experimental data reveals significant differences, particularly in the case of the Schuster's law. These results show that different light conditions affect the distribution of light in a given cultivation system geometry. Consequently, the estimated values of the model parameters will vary accordingly to best fit the specific characteristics of each experimental scenario.

Table 3.1. *Estimation of light distribution model parameters under different light conditions.*

Light distribution model		PUEVIT reactor (blue-red light)	200L reactor (white light)
The Lambert-Beer law $I = I_0 e^{-\xi z}$	$\xi(X) = k\,X$	k = 78.58 [m²/kg]	k = 107.90 [m²/kg]
The Schuster's law $I = \frac{I_0 4\alpha}{(1+\alpha)^2 e^{\delta X z} - (1-\alpha)^2 e^{-\delta X z}}$	$\delta = \sqrt{E_a\,(E_a + E_s)}$ $\alpha = \sqrt{\frac{E_a}{E_a + E_s}}$	Ea = 44.44[m²/kg] Es = 81.36 [m⁻¹]	Ea = 107.89 [m²/kg] Es = 0.002 [m⁻¹]

Regarding the measurements taken with blue-red light, it is noteworthy that the estimated parameter E_s in Schuster's law approaches zero, while E_a is almost equal to the attenuation coefficient k in Lamber-Beer law. These results indicate that, at the concentrations studied, the scattering has a negligible effect. Consequently, the Schuster's law becomes identical to the Lambert-Beer law. This observation can be clearly noticed in Figure 3.6, where the fitting of the two models applied are completely overlapped. For the other set of data instead, the fitting curves between the two models exhibit a subtle variation, with the Schuster's law providing a slightly better accuracy compared to the Lambert-Beer law. However, considering the marginal improvement, it is not advantageous to apply a more complex model when the simpler model with a single parameter can already effectively predict the light profile.

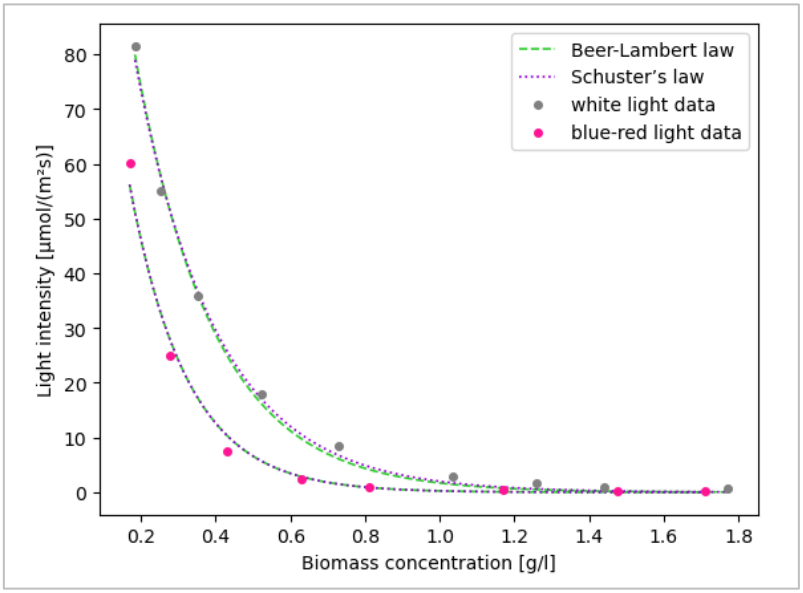

Figure 3.6. *Variation of light intensity with biomass concentration at the end of the tube. Comparison of experimental data (dots), and the corresponding model predictions (dashed lines).*

Overall, based on the obtained results, it can be concluded that for biomass concentrations lower than 2 g/L, the scattering effect can be considered negligible, and the simple Lambert-Beer law is sufficient to model the light distribution within a tubular reactor. Therefore, this expression will be adopted to calculate the average light intensity, which will be subsequently included in the growth model discussed in the following chapter. In fact, as shown above in Figure 3.2 the light regime within the tube is heterogeneous; to overcome this phenomenon, an average irradiance within the entire thickness of the reactor (L) is estimated by integrating the Lambert Beer law over the entire width L.

$$I_{av} = \frac{1}{L}\int_0^L I\,(z)\,dz \tag{3.2}$$

Assuming that biomass is uniformly distributed over the whole reactor volume, the average light intensity within the reactor can be described by:

$$I_{av} = \frac{I_0}{k\,X\,z}\,(1 - e^{-k\,X\,z}) \tag{3.3}$$

Where k is the attenuation coefficient identified earlier by fitting the experimental data, z is the

inlet diameter, I_0 the incident light intensity and X the biomass concentration.

It is crucial to highlight that the value of k is influenced by the concentration and types of pigments present in the microalgae, as they absorb different wavelengths. Therefore, in the second phase of the process considered for this study, when after growing under optimal conditions, microalgae are subjected to stress conditions to induce astaxanthin accumulation, the light profile changes and the k parameter has to be reestimated. Further investigations are needed to examine the impact of nitrogen starvation on the model. A possible approach proposed by Sheng et al. (2018) involves the modeling of light attenuation curves for microalgal suspensions cultivated with various initial nitrate concentrations. Their findings demonstrate that the parameters describing light attenuation in *H. pluvialis* suspension are influenced by astaxanthin content. Similarly, Ma et al. (2022) observed significantly higher estimated attenuation coefficient values under nutrient-limited cultivation compared to nutrient-saturated conditions. This has led to the development of a more complex attenuation model that accounts for light spectra, chlorophyll concentration and carotenoids concentration, which could potentially be adopted for future applications in this study.

Chapter 4

Growth rate modeling

In this chapter the influence of the main factors on *Chromochloris zofingiensis* growth will be investigated adopting the One-Factor-At-a-Time (OFAT) approach. The effect of variables (light intensity, temperature, nitrate and phosphate concentrations) will be assessed individually by monitoring the growth rate while keeping the other factors fixed at their optimal values. The final growth model will be obtained by combining the mathematical expressions that have been developed to characterize the growth response to each analyzed factor.

4.1 Modeling the effects of light intensity

4.1.1 Modeling the biomass growth rate

The growth rate of *C. zofingiensis* has been monitored in a batch system under six different incident irradiances: 30, 50, 70, 100, 120 and 150 μmol/(m² s). The experiments were conducted in a 1 L double-walled bubble column agitated using a magnetic stirrer at speed of 270 rpm. Atmospheric air at a gas flow rate of 1.5 L h^{-1} was continuously supplied. The inoculum was prepared by pre-cultivation in 200mL shake flasks. The column was placed into a light-proof cabinet and artificially illuminated by a LED panel providing a combination of blue and red light. The temperature was kept constant at its optimal value of 25°C using a circulating water thermostat. Samples were collected two or three times per day and the biomass concentration was determined by measuring the optical density at 750 nm using a spectrophotometer. The relationship between OD_{750} and biomass concentration was established by linear regression, using the procedure discussed in § 2.2. Each batch experiment was started with an initial optical density of about 0.2 and has a duration of one week. Figure 4.1 illustrates the growth curves obtained from the six batch cultivations performed. The growth curves demonstrate the typical progression expected for microalgal cultures. In each case, except for the light intensity of 50 μmol/(m² s), an initial lag phase is observed as the microalgae acclimate to the new environmental conditions. However, for the 50 μmol/(m² s) condition, measurements begin at an optical density of 0.4 instead of 0.2, and this difference may account for the distinct trend

observed. At 30 µmol/(m² s) the light intensity is too low, resulting in a final optical density of approximately 0.8 which correspond to a biomass concentration of around 0.72 g/L.

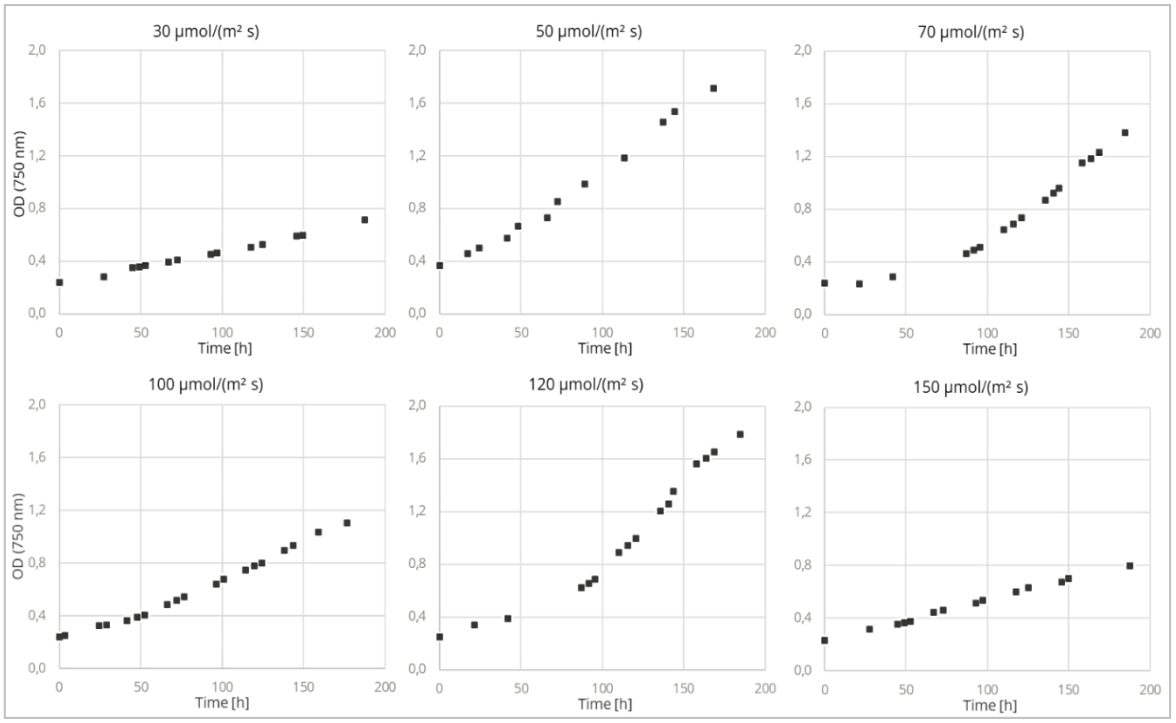

Figure 4.1**.** *Chromochloris zofingiensis growth curves for different incident light intensity.*

As the irradiance gets higher, the growth rate also increases. At 120 µmol/(m² s), the maximum optical density is reached, and the biomass concentration doubles compared to the previous value (1.6 g/L). This observation can be attributed to the characteristic shading effect experienced by phototrophic microorganisms (Metsoviti et al., 2020). When the photon flux density is too low, even low cell densities are sufficient to hinder light to penetrate the whole reactor thickness, and cells located at the back of the cultivation chamber do not receive any photons for photosynthesis. Consequently, the final biomass concentration remains low at low incident photon flux density. Increasing the light beyond the optimal value results again to a decrease of the final biomass concentration. In fact, when the light intensity becomes too high, the cells respond by reducing the number of lamellae in their chloroplasts, promoting lipid accumulation (Juneja et al., 2013) and reducing chlorophyll content with a consequent reduction of the photosynthetic activity. Therefore, to optimize biomass productivity, the ideal approach would be to maintain the average light intensity inside the reactor at its optimal value. This can be achieved by gradually increasing the incident light intensity as the biomass concentration increases. Measurements obtained at 100 µmol/(m² s) deviate from the typical

trend described above and will not be considered in the study. Although the growth curve trend initially appears similar to that obtained at 120 µmol/(m² s) for the first 100 hours, thereafter a significant decrease in the growth rate is observed. This unusual behaviour may be attributed to the occurrence of contamination. In order to evaluate radiation levels causing light-limited growth, photosaturation and photoinhibition phenomena, the growth rate for each light intensity applied was estimated by identifying the exponential phase of the growth curve in Figure 4.1 and by applying the following Equation 4.1:

$$\mu = \frac{ln\, X_2 - ln\, X_1}{t_2 - t_1} \tag{4.1}$$

where X_2 and X_1 correspond to biomass concentration (in g/L) at times t_2 and t_1 (in days), the end and beginning of the exponential growth phase, respectively.

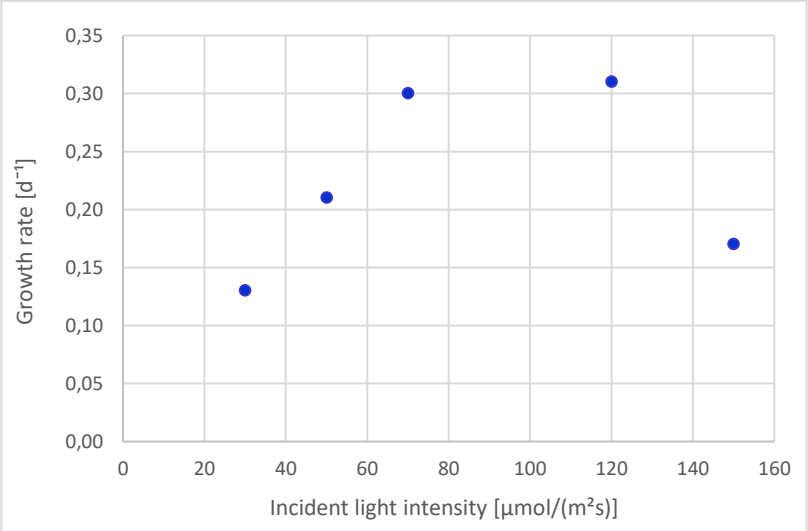

Figure 4.2. *Effect of incident light intensity on phototrophic growth of C. zofingiensis in a bubble column.*

The photosynthesis versus irradiance (P–I) curve obtained is presented in Figure 4.2. As expected from the previous graphs, the growth rate increases with light intensity until it reaches an optimal value of approximately 0.32 h^{-1} at around 100 µmol/(m² s). Beyond this value, a significant photo-inhibitory effect is observed, resulting in a sharp decline in growth rate. To accurately fit the experimental data obtained, several growth kinetic models accounting for photoinhibition at high irradiance have been proposed. Complex models, such as the Camacho Rubio model mentioned earlier (Camacho Rubio et al., 2003), have not been considered in this

analysis; although these models are capable of fitting accurately the data, their high number of parameters introduces the risk of overfitting, leading to poor generalization and performance on new data. The growth models selected are the Lee's model (Lee et al., 1987), the Steele's model (1962), the Muller-Fuega's model (1999) and the Bernard and Remond's model (2012). The results are illustrated in Figure 4.3, where a comparison between the growth rates predicted by the different growth models (red curve) and the growth rates obtained from batch experiments (blue dots) is presented.

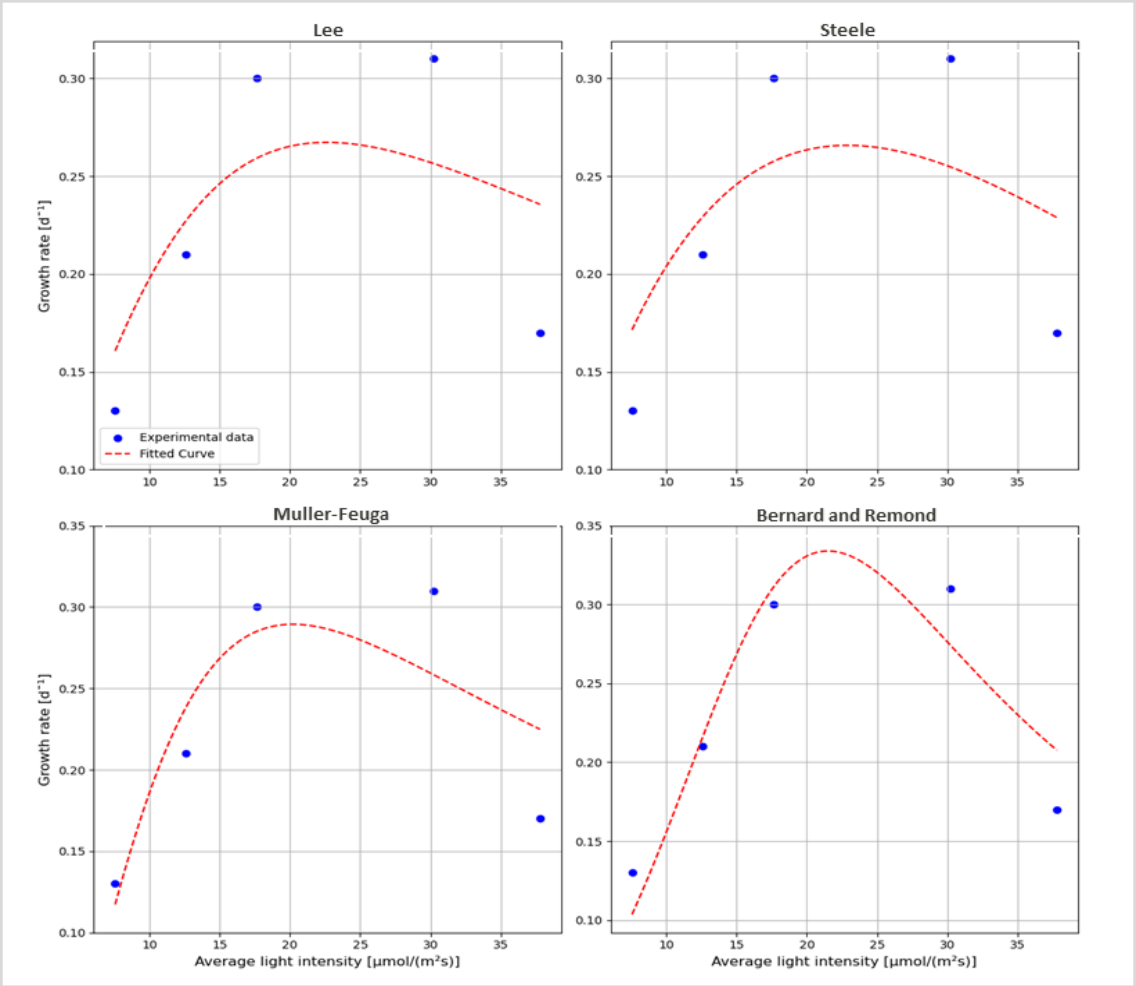

Figure 4.3. *Growth rate of C. zofingiensis in a bubble column as a function of average light intensity. Experimental data have been fitted with various growth models (Table 4.1).*

The growth rate is expressed as function of the average light intensity, which is calculated, as discusses in §3.3, by knowing the incident light intensities, the extinction coefficient, the inner diameter of the bubble column (8 cm) and assuming a constant biomass concentration (specifically the concentration at which the exponential growth phase begins). Among the presented models, Bernard and Remond's model shows the best fit to the experimental data.

Steele's and Lee's model appear to be not suitable to describe light-dependent growth of *C. zofingiensis* and they would seem to be more appropriate for less light-sensitive microalgae species. Muller-Feuga's model fails to accurately predict the significant decline caused by photoinhibition, and it also involves more empirical parameters that are not entirely biologically justifiable compared to Bernard and Remond's model. Therefore, Bernard and Remond's model was found to be the most suitable solution for describing the growth rate of *C. zofingiensis* in a bubble column batch process. The corresponding kinetic parameters were estimated using the curve_fit function in Python, which optimizes the fitting based on the least-squares method. The parameter values obtained for each model analyzed are provided in Table 4.1 below.

Table 0.1 *Kinetic parameters of C. zofingiensis growth rate as function of average light intensity, identified by non-linear regression of experimental data, for different growth models.*

REFERENCES	MODEL	PARAMETERS	R^2
Lee et al. (1987)	$\mu = \mu_{max} \frac{I}{K_I + K_i I^2}$	μ_{max} = 0.59 d^{-1} Ki = 0.05 µmol^{-1} m^2 s K_I = 25.05 µmol m^{-2} s^{-1}	0.6
Steele et al. (1962)	$\mu = \mu_{max} \frac{I}{I_{opt}} e^{\left(1-\frac{I}{I_{opt}}\right)}$	μ_{max} = 0.27 d^{-1} I_{opt} = 22.89 µmol m^{-2} s^{-1}	0.59
Muller-Fuega et al. (1999)	$\mu = 2\,\mu_{max} \frac{(1-\frac{I_e}{I_{opt}})(\frac{I}{I_{opt}}-\frac{I_e}{I_{opt}})}{\left(1-\frac{I_e}{I_{opt}}\right)^2 + \left(\frac{I}{I_{opt}}-\frac{I_e}{I_{opt}}\right)^2}$	μ_{max} = 0.29 d^{-1} I_{opt} = 20.20 µmol m^{-2} s^{-1} I_e = 4.16 µmol m^{-2} s^{-1}	0.73
Bernard and Remond et al. (2012)	$\mu = \mu_{max} \frac{I}{I + \frac{\mu_{max}}{\alpha}\left(\frac{I}{I_{opt}}-1\right)^2}$	μ_{max} = 0.33 d^{-1} I_{opt} = 21.86 µmol m^{-2} s^{-1} α = 0.01 m^2 s µmol^{-1} d^{-1}	0.86

4.1.2 Modeling the oxygen production

In the last decades, the estimation of kinetic parameters from photorespiratory data has been widely adopted (Sforza et al., 2020; Franke et al., 2022). This alternative approach has been employed to further investigate the effect of light intensity and validate the results obtained in §4.1, where each experiment under different light condition was conducted a single time and thus the reliability of the data obtained is questioned. Photorespirometry experiments were performed in a 500 mL double-walled bubble column with an inner diameter of 8cm. The column was equipped with an oxygen sensor to monitor the dissolved oxygen concentration DOC. To prevent gas losses via the headspace, the bottle was completely filled with the microalgal suspension at an optical density of 0.5. The suspension was mixed using a magnetic stirrer at a speed of 270 rpm. The DOC measurement was recorded every five seconds by a GMH 3611 oximeter (GWO 3600 probe, GHM Messtechnik GmbH, Remscheid Germany) and the EBS 20 M monitoring software. The temperature was maintained constant at its optimal value (25°C). Respirometric tests were conducted at six different incident light intensities (30, 50, 70, 100, 120, 150 µmol/(m² s)). To provide enough biomass for the respirometry experiments, *C. zofingiensis* was cultivated in a 1 L bubble column under sterile conditions, stirred at 270 rpm, with a gas stream of CO_2–Air (1.5% v/v) supplied and continuously illuminated. A blue-red LED panel was used to provide an incident light intensity of 100 µmol/(m² s) for the experiments conducted at a light intensity less than or equal to this, while for the ones conducted at 120 and 150 µmol/(m² s) the incident light intensity was set to 150 µmol/(m² s). This procedure ensures that microalgae are already acclimated to the highest light tested and will not be subjected to excessive stress. The biomass harvested for each experiment was replaced with fresh medium to ensure the same inoculum conditions (in the exponential phase) for all the experiments. The determination of the photosynthetic oxygen production rate (OPR) and the oxygen consumption rate (OCR) of *C. zofingiensis* was carried out under defined cultivation conditions, specifically at moderate dissolved oxygen concentration (DOC) levels below air saturation. For this purpose, at the beginning of each experiment, the DOC in the bubble column was reduced to approximately 4.5 mgO_2/L by supplying CO_2. Once the system was sealed, the set-up was exposed to alternating light and dark periods and a total of five light-dark cycles, each lasting around 8 minutes, were executed for each experiment. The data of the first light-dark cycle were discarded to account for the adaptation of the cells to the exerted conditions. The DOC during the experiments was maintained within the range of 4.5 to 6.5 mgO_2/L. Figure 4.4 shows the DOC (mg/L) measured by the oxygen sensor during the four

light-dark cycles for each incident light intensities applied.

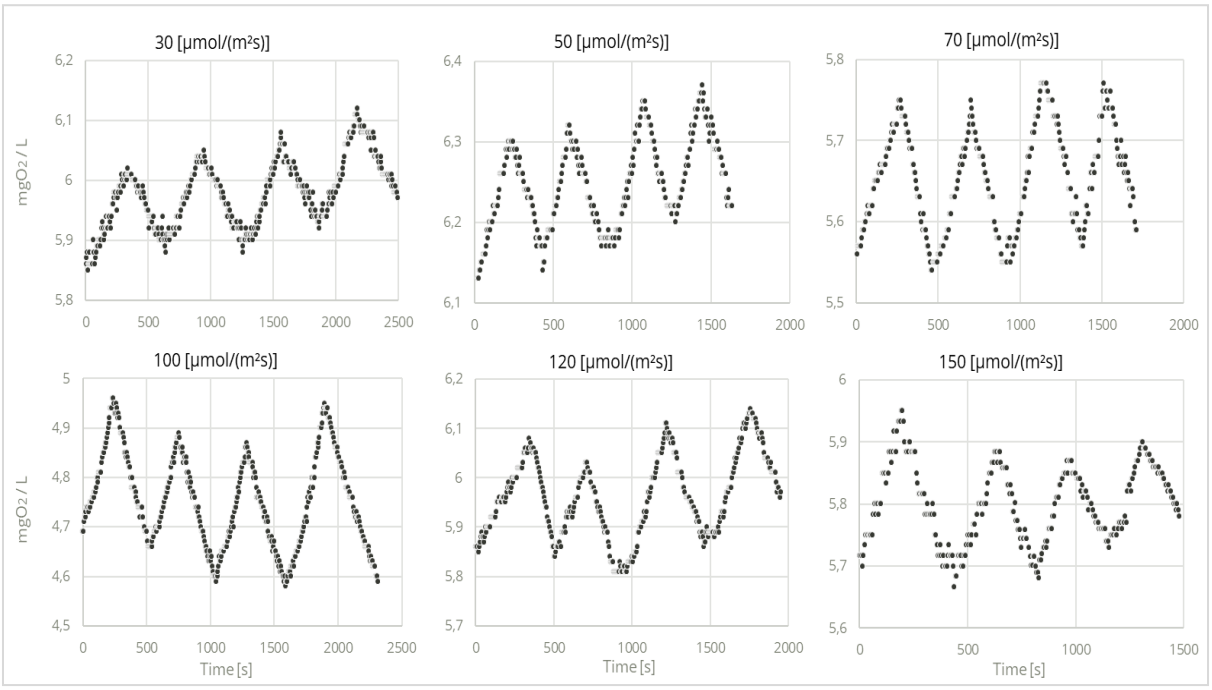

Figure 4.4 *Effect of incident light intensity on dissolved oxygen concentration measured during the four light-dark cycles.*

The estimation of the photosynthetic oxygen production rate during the light period (OPR_L) and the oxygen consumption rate during the dark period (OPR_D) is determined by performing a linear regression analysis on Microsoft Excel. The four slopes obtained for these respective periods were determined and the final OPR_L and OPR_D values were defined as the average between these four slopes. It is worth noting that the slopes of the cycles performed at an incident light intensity of 30 µmol/(m² s) indicate a significant decrease in both oxygen production and consumption compared to the other irradiances tested, proving that the photosynthesis process is light limited. The P-I curve, representing the relationship between light intensity and OPR_{GROSS}, is presented in Figure 4.5. The OPR_{GROSS} was obtained by summing the contributions of OPR_L and OPR_D (Equation 2.1) for each light intensity tested and normalizing the result with respect to the biomass concentration. Experimental data were fitted to the Bernard and Remond's model which has been identified as the most suitable model for predicting *C. zofingiensis* growth rate. The model is described by Equation 4.1, derived by substituting the biomass growth rate in Equation 1.15 with the oxygen production rate.

$$\frac{r_{O_2}}{X} = gOPR = \mu_{maxO_2} \frac{I}{I + \frac{\mu_{maxO_2}}{\alpha}\left(\frac{I}{I_{opt}} - 1\right)^2} \quad (4.1)$$

The parameters were estimated by minimizing the sum of squared errors, following the same procedure described in the previous experiments in §4.1. The resulting value for the maximum specific oxygen rate μ_{maxO2} obtained is 0.44 mgO_2 mgX^{-1} d^{-1} which is related to the biomass maximum specific growth rate μ_{max} by means of a yield factor. The values of the other two parameters I_{opt} and α are 22.64 µmol/(m² s) and 0.019 (m² s/(µmol d)) respectively and are comparable to the ones obtained previously through the conventional batch experiments (I_{opt} = 21.86 µmol/(m² s), α= 0.009 (m² s/(µmol d)).

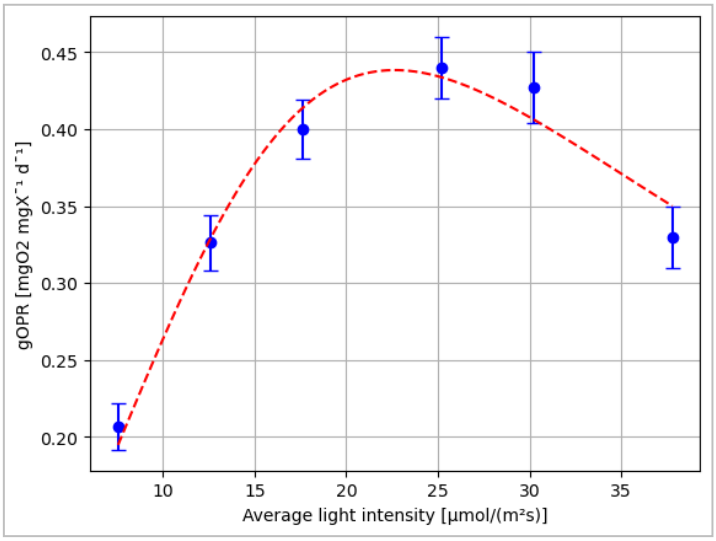

Figure 4.5. *The resulting specific gross OPR (gOPR) as a function of average light intensity. Data fitting was obtained based on the minimization of sum of squared errors adjusting the parameters from Bernard and Remond's model.*

The model successfully fits the experimental data (R^2 = 0.97) and the resulting trend of the P-I curve aligns with previous findings. This further enhances the credibility and reliability of the results obtained. Previous studies have reported that gOPR is directly proportional to the growth rate of *Chlorella vulgaris* (Kazbar et al., 2019). Therefore, based on the biomass generation rate, the corresponding photosynthetic oxygen production rate (r_{O2}) can be identified using the yield factor $Y_{O2/X}$ (Equation 4.2).

$$r_{O_2} = Y_{O_2/X}\, r_X \tag{4.2}$$

The value of $Y_{O2/X}$ for *C. zofingiensis* is not available in the literature. However, based on similar microalgae species, such as *Chlorella vulgaris*, which exhibits properties comparable to *C. zofingiensis*, the $Y_{O2/X}$ value is reported to be 1.5 kg of oxygen per kg of biomass (Kazbar et al., 2019). From the experimental results obtained in this study, the estimated $Y_{O2/X}$ value is 1.4, which aligns reasonably well with the literature value.

One limitation of using photorespirometry to measure the photosynthetic activity as function of light intensity might be that in a few hours of measurement, the effect of acclimation is not captured. Moreover, testing different light conditions on the same biomass within a short time frame may compromise the actual microalgae behavior. This limitation raises concerns about the reliability of photorespirometry, especially when aiming to develop a model applicable to larger-scale systems, such as a tubular reactor. For this reason, the conventional batch growth experiments described above, are supposed to be more suitable for accounting and describing the behavior in long-term steady-state cultivations. However, this study demonstrates that the results obtained through photorespirometry tests align with those obtained from long-term batch cultures. This finding highlights the potential of photorespirometry as an interesting alternative approach, as it offers the advantage of being less time-consuming, allowing for a faster understanding of the effects of light on growth within a few days, as opposed to the several weeks or months required for conventional batch experiments.

4.2 Modeling the effect of temperature

Different photorespirometry tests were conducted also to investigate the effect of temperature on *C. zofingiensis* growth. The same methodology and experimental set-up as in the evaluation of irradiance effects were used. A 500 mL double-walled bubble column completely filled with microalgal suspension with an optical density equal to 0.5 agitated by a magnetic stirrer at 270 rpm and equipped with oxygen sensor was used to monitor the oxygen production and consumption during light-dark cycles. In this case, the focus was on assessing the impact of temperature, which was adjusted for each test using a circulating water thermostat. The incident light intensity instead was fixed at its optimal value which had been determined to be approximately 100 μmol/(m² s). A total of eight respirometric tests were conducted, with

temperatures ranging from 13°C to 31°C (13, 16, 19, 22, 25, 27, 29, 31°C). The biomass used for the tests was acclimated to a light intensity of 100 μmol/(m² s) and a temperature of 25°C, as it had been obtained by cultivating *C. zofingiensis* in a 1 L bubble column under these conditions. To avoid abrupt changes and to limit stress, the respirometry experiments were initiated at a temperature of 25°C. Subsequently, the temperature was gradually increased or decreased to analyze the values below and above the optimal one. A time period of approximately half an hour was allowed between temperature changes before resuming the light-dark cycles and monitoring the photosynthetic activity. Each light-dark cycle had a duration of 10 minutes and was repeated five times for each tested temperature. Data from the first cycle were excluded to account for the acclimation of the microorganisms to the new environmental conditions. Figure 4.6 shows the data collected by the oxygen sensor during the subsequent four light-dark cycles, highlighting how the slopes related to oxygen production and consumption rates are influenced by temperature.

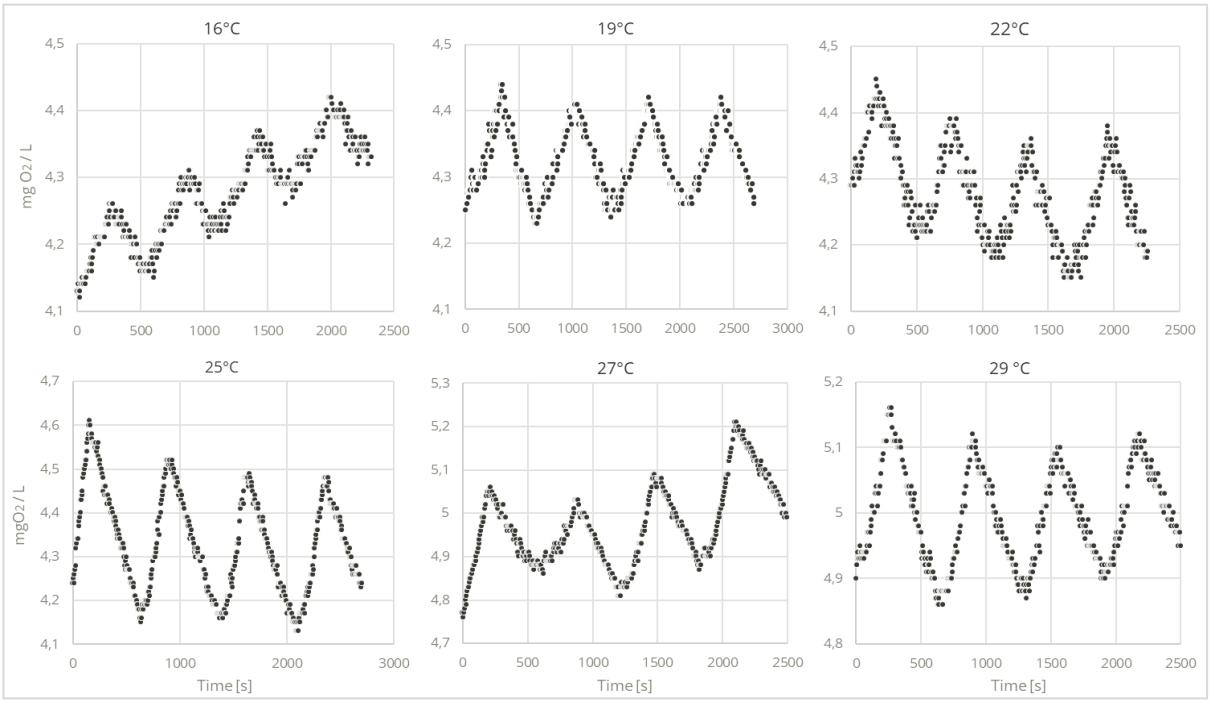

Figure 4.6. *Effect of temperature on dissolved oxygen concentration measured during the four light-dark cycles.*

From the experimental data, it is evident that the slopes of the cycles obtained at 25°C are significantly higher compared to the other temperatures, indicating that the temperature at which the growth of *C. zofingiensis* is maximized will be around this value, in agreement with previous studies (Gorgich et al., 2021). Furthermore, it can be observed that the slopes gradually decrease as the temperature deviates from this value. Specifically, at 25°C the dissolved oxygen

concentration during the light period increases by almost 0.35 mgO_2/L, at 29°C and 22°C it increases by approximately 0.2 mgO_2/L while at 16°C the minimum increase of only 0.15 mgO_2/L was recorded. Each OPR value was calculated as the average of the four slopes obtained. The specific oxygen production rates ($mgO_2/(mgX\ s)$) were estimated by normalization of OPR ($mgO_2/(L\ s)$) with respect to the initial biomass concentration measured (g /L). The model selected to fit the calculated specific oxygen production rates as function of the temperature is the CTMI model (Equation 1.14), which represents a good trade-off between complexity (few parameters with a direct biological interpretation), fit quality and calibration easiness (Grimaud et al., 2017). The model parameters were determined based on the minimization of sum of the squared error (μ_{opt}= 0.41 mgO_2 /(mgX d), T_{min}= 9.07 °C, T_{max}= 30.63 °C, T_{opt}= 26.58 °C) and the resulting temperature values align well with those reported in the literature (Del Campo et al., 2004).

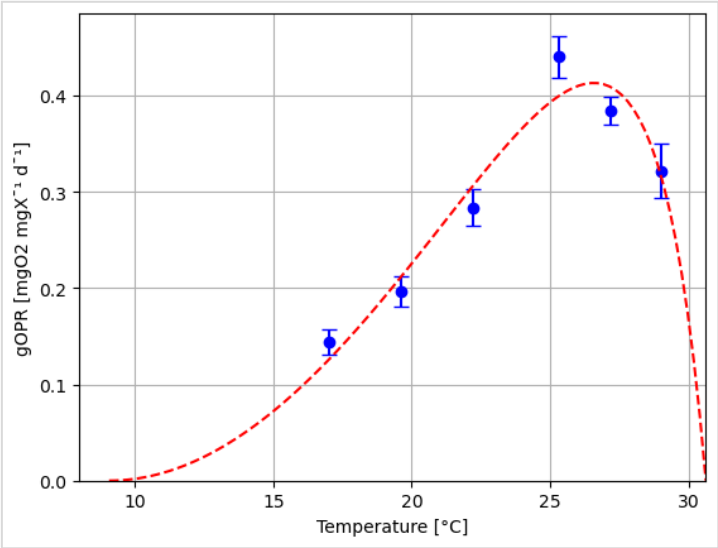

Figure 4.7. *The resulting specific gross OPR (gOPR) as a function of temperature. Data fitting was obtained based on the minimization of sum of squared errors adjusting the parameters from CTMI model.*

The results are reported in Figure 4.7, where the blue points represent the calculated specific gross gOPR and the red curve corresponds to the thermal growth curve obtained by fitting the experimental data through the CTMI model. The model exhibits a good fit with a coefficient of determination R^2 equal to 0.95. *C. zofingiensis* demonstrates a pronounced sensitivity to temperature. The highest growth rate is observed between 25 and 27°C. Therefore, in order to optimize the growth, it is recommended to operate the reactor within this temperature range. Even slight deviations from this optimal range, especially above it, lead to a significant decline

in growth. These findings provide insights into the short-term photosynthetic activity of *C. zofingiensis*, highlighting the immediate impact of temperature changes on growth. To further investigate the effect of temperature, it would be advisable to conduct conventional batch experiments, similar to those carried out for light intensity in §4.1.1, to assess the comparability of the results with those obtained from long-term cultures. Additionally, it would be worthwhile to extend the acclimation period between different conditions to evaluate the extent of its impact on the observed results.

4.3 Modeling the effect of nitrate and phosphate

For this study, a batch experiment was conducted using HD10 Cultivators by CellDEG GmbH. The cultivators (Figure 4.8) were arranged in parallel and placed on a shaking platform, agitated at 350 rpm. The experimental conditions included the supply of atmospheric air enriched with a specific concentration of CO_2 (3% v/v), while maintaining optimal values for light intensity (100 μmol/(m^2 s)) and temperature (25°C). The stock solution consists of $NaNO_3$, K_2HPO_4 and KH_2PO_4 whose concentration has been reported in Table 4.2 as described by Ibanez et al. (2020).

Table 0.1. *Concentrations of Components in the Medium and Calculated Concentrations of Total Phosphate (PO_4), Potassium (K), Nitrate (NO_3), and Sodium (Na).*

Final Concentration (g/L)						
K_2HPO_4	KH_2PO_4	$NaNO_3$	Total PO_4	Total K	NO_3	Na
0,075	0,175	0,750	0,160	0,084	0,550	0,203

The total concentration of nitrate and phosphate in the final solution was determined and considered as the optimal one, since it represents the composition of the culture medium. To evaluate the impact of these two macronutrients on the biomass growth rate, different concentrations of nitrate and phosphate were tested. In order to investigate the effect of nitrogen on the growth of the culture, eight different concentrations were considered (0.05, 0.1, 0.2, 0.3, 0.4, 0.7, 0.85, 1 g/L), five below the optimal value and three above it. The concentration of the other nutrients including phosphate, potassium and sodium were maintained at their optimal level. Similarly, eight different concentrations of phosphate were tested (0.01, 0.05, 0.08, 0.1, 0.12, 0.22, 0.35 g/L) while keeping the other nutrients at their ideal concentration. To ensure

consistent potassium (K) and sodium (Na) levels, potassium chloride (KCl) and sodium chloride (NaCl) were respectively supplied. Each concentration was tested in duplicate. The biomass growth rate was monitored by measuring the optical density (OD) through a spectrophotometer at 750 nm light wavelength. OD measurements were taken twice per day over the course of one week. To accurately determine biomass concentration, a correlation was applied between OD measurements and the actual biomass dry weight, which has been evaluated in previous works as described in §2.2.1 has been applied.

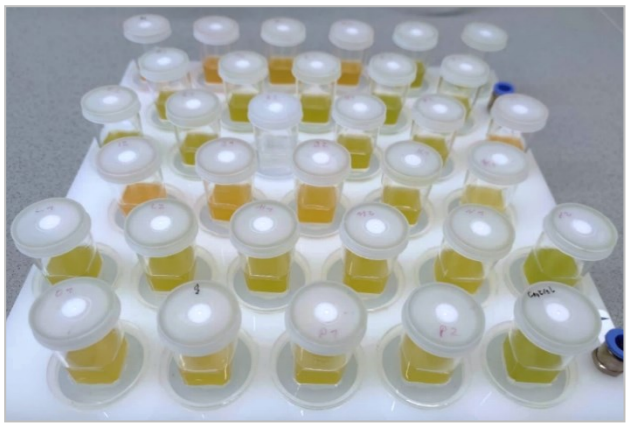

Figure 4.8. *CellDEG HD100 cultivators with C. zofingiensis at different initial nitrate concentration after one week.*

Figure 4.9 shows the change in measured optical density over time for the smallest concentration of nitrate X_N provided (0,05 g/L) and the optimal phosphate concentration X_P. An exponential phase can be identified where a steep linear increase in the plotted data is observed. The growth rate μ (t) was estimated as described for the experiments in §4.1.1 by the previously defined equation (Equation 4.1).

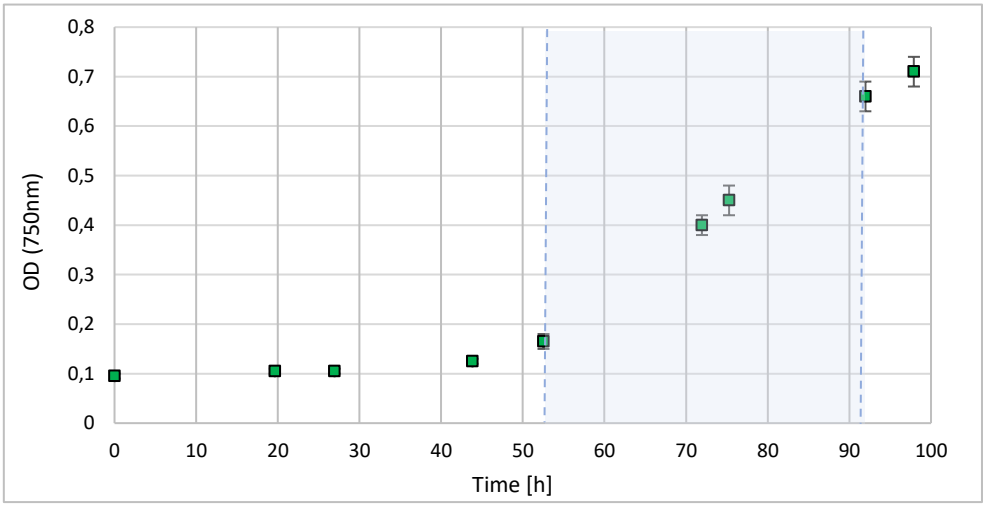

Figure 0.9. *C. zofingiensis growth curve in cellDEG HD100 at optimal light intensity and temperature and the lowest concentration of nitrate tested (0.05 g/L).*

By repeating the experimental procedure for all phosphate and nitrate concentrations considered, the effect of these two macronutrients on biomass growth rate can be investigated. The resulting graphs (Figure 4.10) clearly exhibit a rapid increase in growth rate followed by a plateau, indicating the attainment of the saturation condition. The Monod model (Equation 1.7), which represents the most widely used expression to describe the specific growth rate as a function of nutrient concentrations, was applied to fit the experimental data.

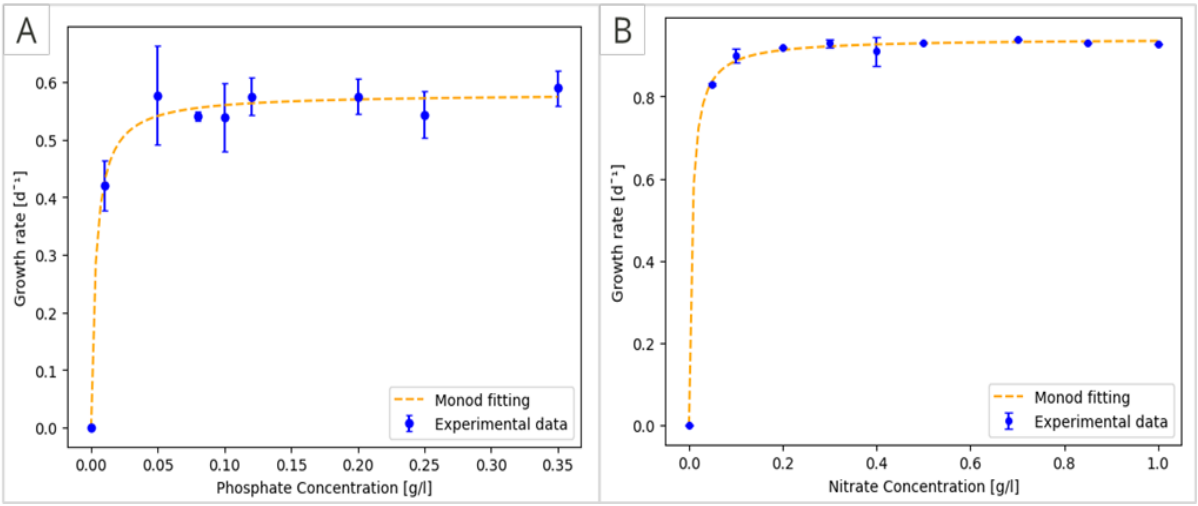

Figure 0.10. *Growth rate of C. zofingiensis as a function of phosphate (A) and nitrate (B) concentration. Data fitting was obtained based on the minimization of sum of squared errors adjusting the parameters from Monod model.*

The curve fitting process to find the parameters of the model that minimize the sum of the squared residuals was performed through the optimization function "curve_fit" in Python. The estimated parameter values are presented in Table 4.3

Table 0.2. *Kinetic parameters of C. zofingiensis growth as function of nitrate and phosphate concentration, identified by non-linear regression of experimental data using the Monod model.*

MODEL	PARAMETERS	R^2
$\mu = \mu_{max} \frac{X_P}{X_P + K_P}$	μ_{max} = 0.580 [d^{-1}] K_P =0.004 [g/L]	0.988
$\mu = \mu_{max} \frac{X_N}{X_N + K_N}$	μ_{max} = 0.941 [d^{-1}] K_N = 0.006 [g/L]	0.999

Based on the results obtained, the Monod model accurately predicts the experimental data, providing insights into how nitrogen and phosphorus concentrations influence *C. zofingiensis* growth rate. In the experiment investigating different nitrate concentrations, it can be noticed that at excessively low concentrations, the algae exhibited signs of stress, manifested by an orange coloration (Figure 4.8). This stress condition has a significant impact on both growth rate and cell composition. However, it is noteworthy that even at concentrations lower than the optimal one present in the growth medium, the growth rate is able to reach the saturated conditions, except for the two lowest concentrations of 0.05 and 0.1 g/L. This suggests that for X_N greater than 0.1 g/L the maximum achievable growth rate is not affected, but rather the time before nutrient limitation and depletion. In the experiment focusing on varying phosphate concentrations, no colour alteration was observed, and growth rate was affected only by using the lowest concentration tested, suggesting that phosphate availability has a lower impact on the algae physiological response compared to nitrate availability. However, it is necessary to repeat these measurements. As evident from the two plots, the maximum growth rates do not coincide as expected. In the graph related to different phosphate concentrations, the obtained trend suggests a lower maximum growth rate compared to the other plot, which appears inconsistent. The expected results should have shown a similar trend, but with saturation conditions reached at μ values equal to those observed in the plot related to X_N. Therefore, to ensure accurate and reliable results, it is essential to repeat the experiment and investigate the discrepancy further. The accurate predictions provided by the Monod model highlight its utility in studying nutrient limitation and its impact on algae growth and physiology. Modeling the effect of macronutrients on the growth rate is crucial for optimizing the production of astaxanthin in *C. zofingiensis.* These findings contribute to our understanding of the complex interactions between nutrient availability and algal growth, enabling the inclusion of these factors in the formulation of the final growth rate expression. By considering nutrient availability alongside other significant influencing factors, such as light, temperature and dissolved oxygen concentration, more accurate predictions for process optimization will be possible.

4.4 Growth rate optimization in tubular reactor

Considering all the mathematical equations applied to predict the influence of light intensity, temperature, nitrate and phosphate concentrations on *C. zofingiensis* growth rate, a

comprehensive growth model is formulated (Equation 4.4). The model is developed assuming that the factors analyzed are independent of each other, as discussed in §1.4. The final rate of photosynthesis is expressed as the product of all the mathematical functions representing the contribution of each factor allowing for a combined assessment of their individual effects on the overall growth dynamics:

$$\mu\,(T\,,I\,,X_N\,,X_P) \;=\; \mu_{max}\;\; \frac{I}{I+\frac{\mu_{max}}{\alpha}\left(\frac{I}{I_{opt}}-1\right)^2}\;\; \frac{X_P}{X_P+K_P}\;\; \frac{X_N}{X_N+K_N}\;\; \phi(T) \qquad (4.3)$$

For the 200L reactor, the initial phase of the process involves concentrations of nitrate and phosphate that correspond to those presented in the BM medium (Table 4.2) and it has been demonstrated that at these concentrations, the growth rate of *C. zofingiensis* is not limited by nutrients. Therefore, the two functions representing the dependency on nitrate and phosphate can be omitted to model the first phase of growth under optimal conditions, but they will need to be considered in the second phase of the process, for modeling the growth of C. zofingiensis under nitrogen starvation conditions. Additionally, the temperature is assumed to be constant since no heat exchanger is used and any oscillations related to ambient temperature are considered negligible. Consequently, during the batch operation of the 200L reactor, the only variable measured and monitored was turbidity, which serves as an indicator of biomass concentration.

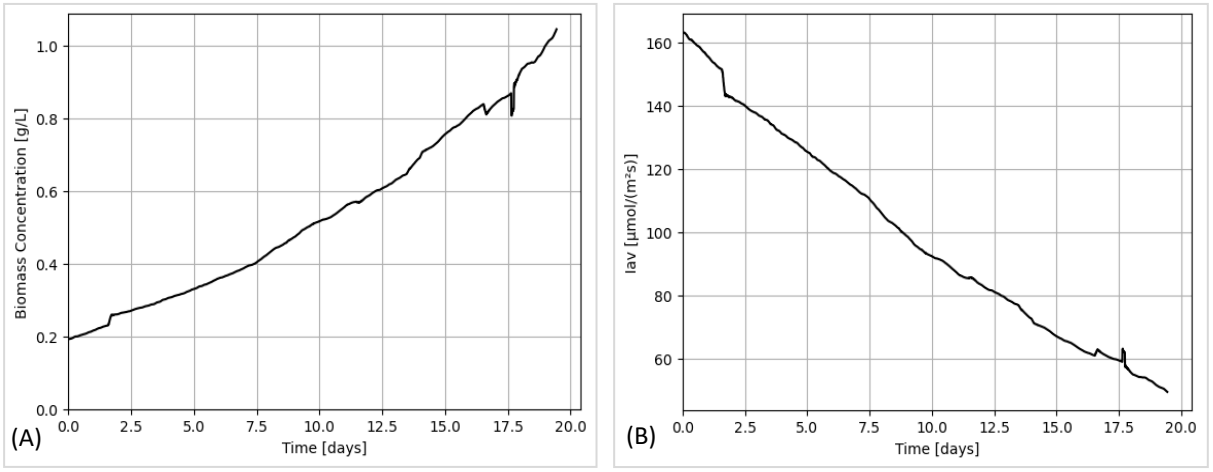

Figure 0.11. *Variation of biomass concentration (A) and average light intensity (B) over time in the tubular reactor.*

To remove outliers, reduce noise, and minimize fluctuations in the data recorded by the turbidity sensor every five minutes, a moving average with a specified window size was applied. This technique helps smooth out the data by replacing each data point with the average of itself and its neighboring points within the window. After smoothing the turbidity data, the change in biomass concentration (g/L) over time was determined by applying the correlation presented in §2.1.3. Throughout this period, the incident light intensity was maintained at a constant level (250 µmol /(m^2 s)). However, due to the increasing biomass concentration, the average light intensity experienced a decrease (Figure 4.11). This decrease was assessed using the Beer-Lambert law, with the extinction coefficient estimated in §3.3 for the specific wavelength and tubes used in the 200L reactor. The calculated average light intensity within the reactor is significantly higher compared to the intensities testes at the laboratory scale. According to the results obtained by monitoring microalgae growth rate in a bubble column in §4.1, the applied incident light intensity is excessively high and limits the growth of *C. zofigiensis*. This could be one of the reasons behind the low growth rate observed; indeed, starting the exponential phase at the same biomass concentration of approximately 0.2 g/L in both the reactor and the 1L bubble column, it takes considerably more time for the 200L reactor to reach the same final biomass concentration, even when considering the lowest light conditions tested with bubble column (Figure 4.1). This is more evident in Figure 4.12 which illustrates the evaluated growth rate throughout the batch operation.

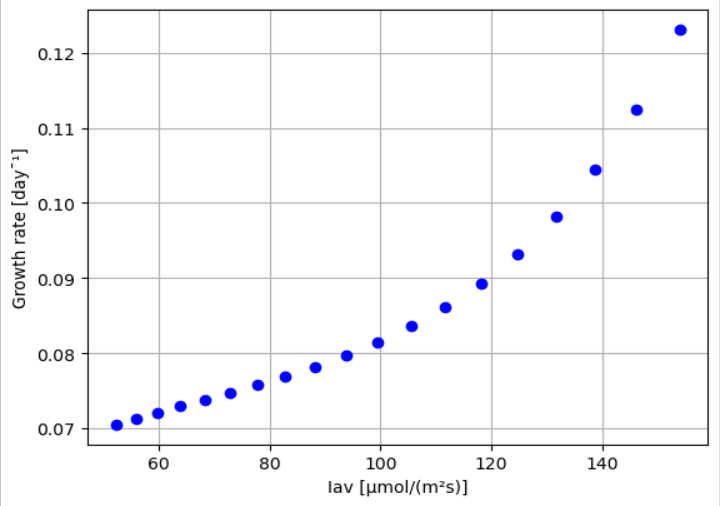

Figure 0.12. *Growth rate values of C. zofingiensis in the tubular reactor calculated daily as function of the average light intensity.*

The growth rates were assessed daily by fitting the data of Figure 4.11 with a polynomial function and applying Equation 4.1 to the resulting regression curve. As expected, the growth rate values obtained in the current study are lower than those obtained in the bubble column (Figure 4.2). While photoinhibition could explain this disparity based on previous experiments, it is important to consider other potential factors that may affect the growth. Monitoring the dissolved oxygen concentration is crucial, as it may also play a role in limiting growth. Additionally, due to the differences in the type and size of the two cultivation systems, it is possible that the turbulence in the reactor is more favorable, allowing for shorter mean durations of light-dark cycles and potentially avoiding photoinhibition even under high incident light intensities. To gain further insights, a comprehensive fluid dynamic study should be undertaken to compare the turbulence experienced by microalgal cells in the two different systems. Figure 4.11 illustrates that as the biomass concentration increases, light penetration into the culture decreases due to light scattering and absorption by cells. This results in reduced light availability for the lower cell layers, leading to a decrease in photosynthetic activity and growth rate (Figure 4.12). In order to prevent a decrease in the average light intensity experienced by individual cells within the culture, it is necessary to increase the incident light intensity during the operation. To accomplish this, further studies should include additional batch experiments conducted under different light conditions. The objective will be to identify the average light intensity that maximizes growth, then maintain this value consistently throughout the batch operation, and evaluate whether it aligns with the optimal intensity identified in the bubble columns. Up to now, two batches were conducted, and the aforementioned results correspond to the batch performed with an incident light intensity of approximately 250 μmol/(m^2 s). During the exponential phase of this batch, a growth rate of approximately 0.8 d^{-1} was observed. The second batch was carried out under the same conditions, except that the incident light intensity was reduced by half (125 μmol/(m^2 s)), resulting in slightly higher growth rate values during the exponential phase, around 0.95 d^{-1}. It is worth noting that while the temperature is assumed to be constant, there is a notable difference in temperature between the two datasets. The second batch was conducted in February, while the first batch was carried out in March, resulting in measured temperatures of approximately 20°C and 25°C, respectively. As indicated by the findings in §4.2 and in previous works (Del Campo et al., 2004), 25°C is nearly the optimal temperature for maximizing *C. zofingiensis* growth. Consequently, the batch conducted in February was further away from the optimal temperature compared to the other one and it would likely exhibit even greater growth under the same temperature conditions.

Chapter 5

Oxygen accumulation in photobioreactors

It is widely known that high dissolved oxygen concentrations (DOC) can inhibit microalgal growth. Inhibition by high DOCs depends on cultivation conditions and exposure duration and varies for different strains. High amounts of oxygen can be accumulated especially in tubular photobioreactors due to the low gas-liquid mass transfer efficiency of this cultivation system that can lead to extensive spatial gradients of oxygen along the tube axis (§1.2.1). Therefore, in the following sections, photorespitometry experiments have been conducted to investigate the impact of high dissolved oxygen concentration on the growth of *C. zofingiensis* and contribute to the development of strategies to optimize cultivation conditions and to increase productivity.

5.1 Experimental set-up

The photorespirometry protocol applied in this study is based on a procedure developed and refined by Sforza et al. (2019, 2020) which consists of two phases. In the first phase, microalgal cells are exposed to intermittent light-dark illumination cycles following a similar procedure used for analyzing the effect of light intensity and temperature (§4.1 and §4.2): five alternating light-dark illumination cycles, lasting approximately 10 minutes each, with data from the first cycle discarded. The aim of this phase is to establish the basal oxygen production and consumption rate below saturation conditions, at moderate dissolved oxygen concentrations (between 4-7 mgO_2/L). To achieve this, the DOC in the bubble column is initially lowered to around 3 mgO_2/L by supplying CO_2. In the second phase, the light is continuously provided until a constant dissolved oxygen value is reached within the system. The oxygen production rate (OPR) can be determined by analyzing the temporal change in DOC during the continuous light phase, calculating the differential quotient dC_{O2}/dt over time intervals of approximately 10 minutes (Equation 2.4). Once the saturated condition is reached, an additional phase has been introduced to the conventional protocol during which CO_2 is supplied to decrease the DOC back to the initial value, and the light/dark cycles are repeated to assess whether photosynthetic

activity is affected once saturation conditions are reached, despite no longer being in such conditions. The photorespirometric tests have been conducted in a 500 mL double-walled bubble column, agitated at 270 rpm, at constant optimal values of light intensity (100 μmol/(m² s)) and temperature (25°C). The pre-inoculum was cultivated in a 1 L bubble column under the same light and temperature conditions, and fresh medium was periodically added in order to maintain it at the same conditions (exponential growth phase) for each experiment. The tests were performed for five different optical densities (0.2, 0.5, 0.8, 1 and 1.5) selected to the range of concentrations that are typically attained during cultivation processes of *C. zofingiensis* in the 200L tubular reactor. Since each experiment lasted only a few hours, it was assumed that the optical density remained constant throughout the duration of the experiment.

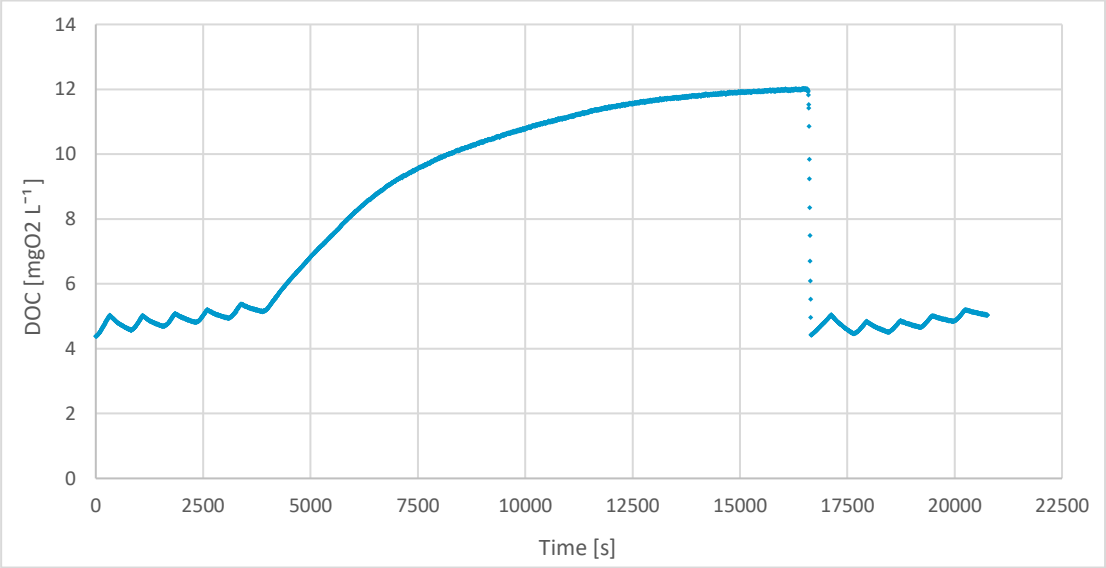

Figure 5.1. *Respirometric protocol example performed at optical density of 0.2.*

5.2 Results

Figure 5.1 illustrates the dissolved oxygen concentration data collected during the experiment at optical density of 0.2. It can be observed that above a dissolved oxygen concentration of 7 mgO_2/L, with the increasing of exposure duration and higher DOCs, the increment of DOC gradually slows down, until it eventually becomes zero at the maximum DOC. The second phase lasts about 4 hours, and the saturation conditions are reached for a DOC of approximately 12 mgO_2/L. Comparing the two sets of light-dark cycles, it is evident that even before calculating the oxygen production rate (OPR), the slopes observed after reaching the saturation

condition are slightly lower than those observed before it, thus providing clear evidence of the impact of oxygen accumulation on the growth rate of *C. zofingiensis*. This is better illustrated in Figure 5.2 where the two sets of executed light-dark cycles are presented in the same plot for a more straightforward and immediate comparison. During the light phase, the dissolved oxygen concentration increases by approximately 0.4 mgO_2/L in 4 minutes in the cycles obtained at the beginning of the experiment, while it increases by around 0.3 mgO_2/L in the cycles executed once the saturation conditions have been reached. The consumption of oxygen during the dark phase also appears to be lower in the latter case: in 8 minutes the dissolved oxygen concentration decreases by approximately 0.3 mgO_2/L and 0.15 mgO_2/L in the first and second case respectively. Since the specific gross OPR is calculated by summing the contribution of the OPRs during the light and dark phases, the values evaluated after reaching the saturation condition will naturally be lower, indicating that the cells have been affected by the previous oxygen accumulation.

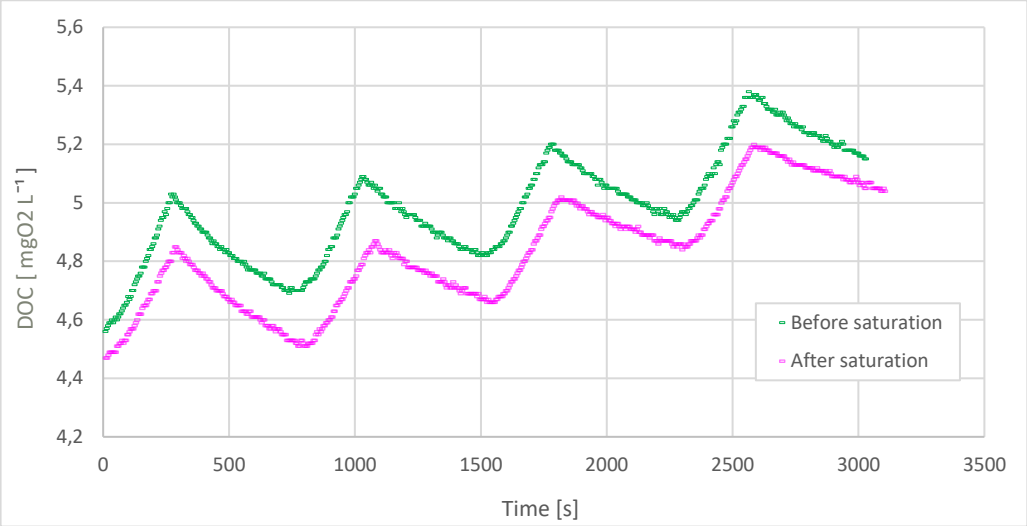

Figure 5.2. *Comparison between the four light-dark cycles executed before and after reached the saturation condition at optical density of 0.2.*

The OPRs were determined using the same methodology as described in the previous experiments, which involved assessing the positive and negative slopes for each cycle and calculating the average of the four obtained results. The results are presented in Figure 5.3 as histograms where each bin represents the gross OPR, composed of a yellow section and a blue section representing the two contributions OPR_L and OPR_D, respectively. The biomass concentration was determined by multiplying the optical density considered by 0.9 in accordance with the linear correlation obtained in previous works as described in §2.2.1.

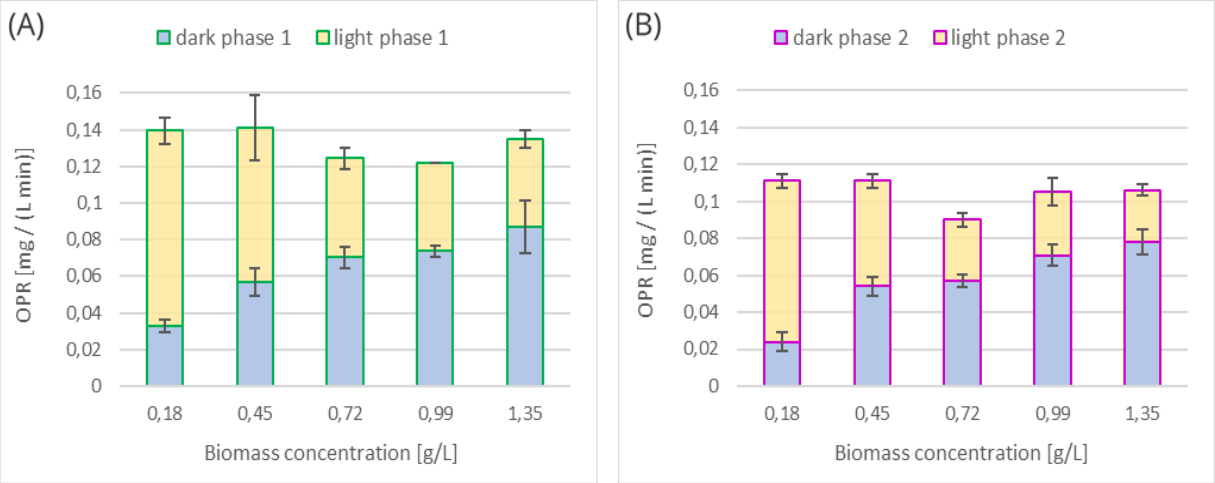

Figure 5.3. OPR_L (yellow) and OPR_D (blue) calculated are reported as a function of biomass concentration before (A) and after (B) reached the saturation condition.

Comparing the sets of light-dark cycles represented in the two histograms, as mentioned above, it appears that gross OPR values decrease in the second set of cycles executed after reaching the saturated condition. Both OPR_L and OPR_D are affected by the previous oxygen accumulation, but the impact is more significant on the oxygen production during the light phase. In theory, as the biomass concentration increases, more cells are available for photosynthetic activity, leading to an expected increase in both oxygen production and consumption. However, a higher concentration of algae results in a lower average light intensity, which can potentially limit photosynthesis, especially if the system is not adequately agitated. Microalgae require sufficient light energy for photosynthesis to occur efficiently and when the light intensity becomes too low, the photosynthetic rate may reach a maximum level and remain constant, even with higher biomass concentrations. This phenomenon is evident in the plots, where it can be observed that during the light period, oxygen production decreases with increasing biomass concentrations until around 0.7 g/L. Beyond this point, further increases in biomass concentration do not significantly affect the oxygen production rate (OPR_L), which remains relatively constant. In contrast, during the dark period, there is a progressive increase in oxygen consumption (OPR_D) with increasing biomass concentration.
The OPR when light was provided continuously has been assessed by considering time intervals of approximately 8 minutes in order to approximate the curve into several lines for which by linear regression evaluate the slope.

By assigning the corresponding DOC measured at the beginning of the respective time interval for each value of OPR evaluated, the decrease of the OPR over increasing DOCs can be plotted. For a better comparison, the experimentally obtained OPR data were normalized on the OPR

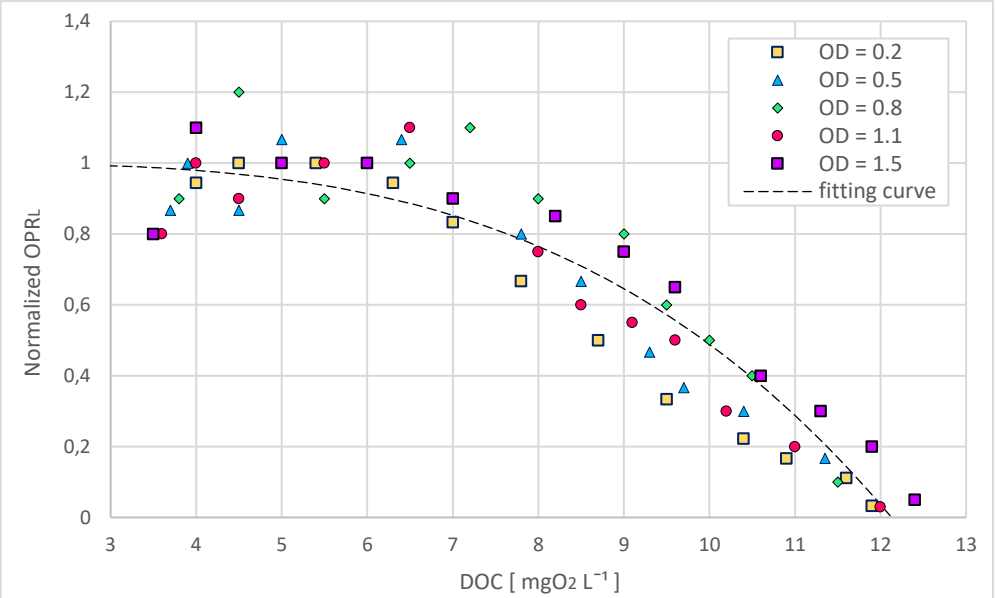

Figure 5.4. *Normalized OPR of C. zofingiensis over increasing dissolved oxygen concentrations at different cultivation conditions. The data were collected in the continuous light phase of respirometry experiments.*

reference values that were calculated during the first phase of the respective experiment, and the results are reported in Figure 5.4. The trends are quite similar among the five biomass concentrations analyzed. Up to approximately 6 mgO_2/L, the OPR_L remains relatively constant, however, beyond this point, the OPR_L starts to decrease and reaches zero at around 12 mgO_2/L. Experimental data could be described using the following model (Equation 5.1) proposed by Costache et al. (2013):

$$OPR_L = 1 - \left(\frac{C_{O_2}}{K_{O_2}}\right)^n \tag{5.1}$$

In this equation, K_{O2} is the oxygen inhibition constant, C_{O2} is the dissolved oxygen concentration and n is a form parameter. By fitting the experimental data to this equation, the characteristic parameter values were determined ($K_{O2} = 12.02$ mg/L, $n = 3.44$), verifying that the model can simulate the inhibitory response to DOC.

It is crucial to verify that the DOC measure inside the 200L reactor does not exceed the value of 12 mgO_2/L and preferably remains below 9 mgO_2/L to minimize the impact on the

photosynthetic rate. If the DOC exceeds these thresholds, measures to enhance gas-liquid mass transfer efficiency and prevent oxygen accumulation should be implemented. One possible solution is to increase the gas flow rates; nevertheless, it should be considered that high gas flow rates can induce shear stress on the cells and result in significant energy costs. Another approach is to incorporate a degassing unit that removes oxygen from the culture through air or CO_2 stripping. However, solely relying on degassing units would only create optimal growth conditions immediately after the degassing system, as concentration gradients of increasing DOCs would emerge along the lengths of the tubular photobioreactors. Another solution could involve increasing the gas-liquid interface. In this regard, ongoing research is focusing on exploring several alternative tools such as hollow fiber modules and porous membrane systems that can be integrated into the tubes of the photobioreactors (tPBRs).

Conclusions

This thesis focuses on optimizing the growth of *C. zofingiensis*, a unicellular microalga that is gaining attention for its robust growth and its ability to co-produce high levels of lipids, particularly triacylglycerols (TAGs), and value-added products including the powerful antioxidant astaxanthin, representing a promising strategy to improve production economics and facilitate industrial-scale implementation. In order to maximize the growth, the impact of key factors was investigated at laboratory scale using the One-Factor-At-a-Time (OFAT) approach. the optimal values of average light intensity, temperature, phosphate and nitrate concentration were determined and a growth model accounting for the contribution of all these factors was developed. The experimental data analysed were obtained through a series of conventional batch experiments and photorespirometry, which proved to be a valuable tool for quickly assessing the impact of these factors on the microalga's photosynthetic activity. The distribution of light was accurately modelled using the Beer-Lambert law, indicating that under the considered conditions of light and biomass concentration, the scattering effect can be neglected. However, it is crucial to note that the developed model cannot be directly applied to the second stage of the process, while working under stress condition, as the extinction coefficient value is influenced by the concentration and types of pigments present in the microalgae. Thus, further investigations are needed to examine the impact of nitrogen starvation on the model. The optimal conditions determined in the laboratory will have to be applied to the 200L reactor to assess the possibility of adopting the model also on an industrial scale. During this study, the first two batch experiments were conducted on the 200L reactor showing a significantly lower growth rate than that obtained in the bubble columns. This discrepancy could be attributed to various factors, including the distinct geometry of the system, which can lead to different levels of turbulence, as well as the potential occurrence of oxygen accumulation commonly observed in tubular reactors. Therefore, for future studies, it is recommended to conduct a comprehensive fluid dynamic study to investigate the turbulence experienced by microalgal cells in the 200L reactor and it is suggested to include DOC monitoring in future studies, by employing two sensors placed at the reactor inlet and outlet to account for potential spatial gradients of oxygen along the tube. The results obtained in this study suggest the importance of maintaining the DOC below 9 mgO_2/L to prevent a significant

decrease in growth and to avoid reaching saturation conditions (around 12 mgO_2/L), as it was demonstrated that microalgal cells experience adverse effects once saturation is reached. Moreover, to further optimize growth during continuous light operation, it is recommended to use the light distribution model obtained in this study to increase the incident light intensity during operation and maintain a constant average light level in the culture medium as biomass concentration increases. To ensure the applicability of the developed model at a larger scale, further batch experiments in the 200L reactor under different lighting conditions, following the methodology employed for the bubble columns, should be conducted to identify the optimal average light intensity that maximizes growth and verify its consistency with the findings observed at the laboratory scale. Overall, this study provides valuable insights into optimizing the growth conditions of *C. zofingiensis.* The recommendations and findings presented here lay the foundation for future research and potential implementation of these strategies at an industrial scale, thus contributing to the advancement and sustainability of microalgae-based production.

References

Ahmad, I., Abdullah N., Koji, I., Yuzir, A., Muhammad, S. E. (2021). Evolution of Photobioreactors: A Review based on Microalgal Perspective, *IOP Conf. Ser.: Mater. Sci. Eng*., **1142,** 012004.

Aiba, S. (1982). Growth kinetics of photosynthetic microorganisms: in microbial reactions. *Adv. Biochem. Eng.*, **23,** 85–156.

Alaswad, A., Dassisti M., Prescott T., Olabi A.G. (2015). Technologies and Developments of Third Generation Biofuel Production. *Renew. Sustain. Energy Rev*., **51**, 1446–1460.

Aljabri, H., Cherif, M., Siddiqui, S.A., Bounnit, T., Saddaoui, I. (2023). Evidence of the drying technique's impact on the biomass quality of *Tetraselmis subcordiformis* (Chlorophyceae). *Biotechnol. Biofuels,* **16**, 85.

Atiku A., Mohamed R.M.S.R., Al-Gheethi A.A., Wurochekke A.A., Kassim A.H. (2016). Harvesting microalgae biomass from the phycoremediation process of greywater. *Environ. Sci. Pollut. Res.,* **23**, 24624–24641.

Bannister, T. (1979). Quantitative description of steady state, nutrient-saturated algal growth, including adaptation. *Limnol. Oceanogr*., **24**, 76–96.

Béchet, Q., Shilton, A., Guieysse, B., (2013). Modeling the effects of light and temperature on algae growth: State of the art and critical assessment for productivity prediction during outdoor cultivation. *Biotechnol. Adv*., **31**, 1648–1663.

Benner, P., Meier, L., Pfeffer, A., Krüger, K., Oropeza Vargas, J.E., Weuster-Botz, D. (2022). Lab-scale photobioreactor systems: principles, applications, and scalability. *Bioprocess Biosyst. Eng*., **45**, 791–813.

Bernard, O., Rémond, B., (2012). Validation of a simple model accounting for light and temperature effect on microalgal growth. *Bioresour. Technol*., **123**, 520–527.

Blanken W., Postma, P.R., De Winter, L., Wijffels, RH, Janssen, M. (2016). Predicting microalgae growth. *Algal Res.,* **14**, 28–38.

Borowitzka, M. A., Vonshak, A. (2017). Scaling up microalgal cultures to commercial scale. *Eur. J. Phycol.,* **52**, 407–18.

Carney, L.T., Lane, T.W. (2014). Parasites in algae mass culture. *Front. Microbiol*., **5**, 278.

Chalker, B.E. (1980). Modeling light saturation curves for photosynthesis: an exponential function. *J. Theor. Biol.*, **84**, 205–215.

Chandra, R., Iqbal, H.M.N., Vishal, G., Lee, H.S., Nagra, S. (2019). Algal biorefinery: a sustainable approach to valorize algal-based biomass towards multiple product recovery. *Bioresour. Technol*., **278**, 346-359.

Chanquia S.N., Vernet, G., Kara, S. (2022). Photobioreactors for cultivation and synthesis: Specifications, challenges, and perspectives. *Eng Life Sci.,* **22**, 712–724.

Chen, J., Wei, D., Pohnert, G. (2017). Rapid estimation of astaxanthin and the carotenoid-to-chlorophyll ratio in the green microalga Chromochloris zofingiensis using flow cytometry. *Mar. Drugs*, **15**, 231.

Chisti Y. (2007). Biodiesel from microalgae. *Biotechnol. Adv.,* **25**, 294– 306.

Chowdury, K.H., Nahar, N., Deb, UK. (2020). The Growth Factors Involved in Microalgae Cultivation for Biofuel Production: A Review. *Comput. Water Energy Environ. Eng.,* **9**, 185-215.

Chu F.F., Chu P.N., Cai P.J., Li W.W., Lam P.K.S., Zeng R.J. (2013). Phosphorus plays an important role in enhancing biodiesel productivity of Chlorella vulgaris under nitrogen deficiency. *Bioresour. Technol.* **134**, 341–346.

Cornet, J.F., Dussap, C.G., Gros, J.B., Binois, C., Lasseur, C. A. (1995). A simplified monodimensional approach for modeling coupling between radiant light transfer and growth kinetics in photobioreactors. *Chem. Eng. Sci.,* **50**, 1489–1500.

Darvehei P., Bhri P.A., Moheimani N.R. (2018). Model development for the growth of microalgae: A review. *Renew. Sust. Energ. Rev*., **97**, 233–258.

Del Campo, J.A., Rodríguez, H., Moreno, J., Vargas, M.A., Rivas, J., Guerrero, M. G., (2004). Accumulation of astaxanthin and lutein in Chlorella zofingiensis (Chlorophyta). *Appl. Microbiol. Biotech.,* **64**, 848–854.

Dermoun, D., Chaumont D., Thébault, J.M., Dauta A. (1992). Modelling of growth of Porphyridium cruentum in connection with two interdependent factors: light and temperature. *Bioresour. Technol.,* **42**, 113–117.

Dienst, D., Wichmann, J., Mantovani, O., Rodrigues, J.S., Lindberg, P. (2020). High density cultivation for efficient sesquiterpenoid biosynthesis in *Synechocystis* sp. PCC 6803. *Sci Rep,* **10**, 5932.

Ding, N., Li, C., Wang, T., Guo, M., Mohsin, A., Zhang, S. (2021). Evaluation of an enclosed airlift photobioreactor (ALPBR) for biomass and lipid biosynthesis of microalgal cells grown under fluid-induced shear stress. *Biotechnol. Biotechnol. Equip.,* **35**, 139–149.

Dönz OC. (1934) Chlorella zofingiensis, eine neue Bodenalge. *Ber. Schweiz. Bot. Ges.,* **43**, 127–31.

Eilers, P.H.C., Peeters, J.C.H. (1988). A model for the relationship between light intensity and the rate of photosynthesis in phytoplankton. *Ecol. Model.,* **42**, 199–215.

Fakhri, S., F. Abbaszadeh, L. Dargahi, M. Jorjani (2018). Astaxanthin: A mechanistic review on its biological activities and health benefits. *Pharmacol. Res.,* **136**, 1-20.

Feng, P., Deng, Z., Fan, L., Hu, Z. (2012). Lipid accumulation and growth characteristics of Chlorella zofingiensis under different nitrate and phosphate concentrations. *J. Biosci. Bioeng.,* **114**, 405–410.

Franke, S., Steingröwer, J., Walther, T., & Krujatz, F. (2022). The Oxygen Paradigm—Quantitative Impact of High Concentrations of Dissolved Oxygen on Kinetics and Large-Scale Production of Arthrospira platensis. *ChemEng*., **6**, 14.

Fučíková, K., Lewis, L.A. (2012). Intersection of Chlorella, Muriella and Bracteacoccus: Resurrecting the genus Chromochloris Kol et Chodat (Chlorophyceae, Chlorophyta). *Fottea*. **12**, 83–93.

Gorgich, M., Martins, A., Mata, T., Caetano, N. (2021). Composition, Cultivation and Potential Applications of Chlorella Zofingiensis – a Comprehensive Review. *Algal Res*., **60**, 102508.

Grima, E.M., J.M. Sevilla, J.A. Pérez, F.G. Camacho (1996). A study on simultaneous photolimitation and photoinhibition in dense microalgal cultures taking into account incident and averaged irradiances. *J. Biotechnol*. **45**, 59–69.

Grimaud, G. M., Mairet, F., Sciandra, A., Bernard, O. (2017). Modeling the temperature effect on the specific growth rate of phytoplankton: a review. *Rev. Environ. Sci. Biotechnol.,* **16**, 625–645.

Heining, M., Sutor, A., Stute, S. C., Lindenberger, C. P., & Buchholz, R. (2015). Internal illumination of photobioreactors via wireless light emitters: a proof of concept. *J. Appl. Phycol.,* **27**, 59–66.

Hobuss, C.B., Rosales, P.F., Venzke, D., Souza, P.O., Gobbi, P.C., Gouvea, L.P., Santos, M.A., Pinto, E., Jacob-Lopes, E. and Pereira, C.M., (2011). Cultivation of algae in photobioreator and obtention of biodiesel. *Rev. Bras. Farmacogn.,* **21**, 361–364.

Huang, Q., Jiang, F., Wang, L., Yang, C. (2017). Design of photobioreactors for mass cultivation of photosynthetic organisms. *Eng*., **3**, 318–329.

Huang, J., Feng, F., Wan, M., Ying, J., Li, Y., Qu, X., Pan, R., Shen, G., & Li, W. (2015). Improving performance of flat-plate photobioreactors by installation of novel internal mixers optimized with computational fluid dynamics. *Bioresour. Technol*., **182**, 151–159.

Juneja, A., Ceballos, R., Murty, G., (2013). Effects of Environmental Factors and Nutrient Availability on the Biochemical Composition of Algae for Biofuels Production: A Review. *Energies,* **6**, 4607–4638.

Ibañez, M.V., Leonardi, R.J., Heinrich, J.M., Steingroewer, J., Walther, T. and Felix, K., (2020). A Rapid Assessment of the Radiative Properties from a Suspension of Chromochloris Zofingiensis. *J. Photochem. Photobiol*., **3-4**, 100007.

Kamravamanesh, D., Kiesenhofer, D., Fluch, S., Lackner, M., Herwig, C., (2019). Scale-up challenges and requirement of technology-transfer for cyanobacterial poly (3-hydroxybutyrate) production in industrial scale. *Int. J. Biobased Plast.,* **1**, 60-71.

Kazbar, A., G. Cogne, B. Urbain, H. Marec, B. Le-Gouic, J. Tallec, H. Takache, A. Ismail, J. Pruvost (2019). Effect of dissolved oxygen concentration on microalgal culture in photobioreactors. *Algal Res*., **39**, 101432.

Kim S., Park J.E., Cho Y.B., Hwang S.J. (2013). Growth rate, organic carbon, and nutrient removal rates of Chlorella sorokiniana in autotrophic, heterotrophic, and mixotrophic conditions. *Bioresour. Technol*., **144**, 8-13.

Klok, J., Verbaanderd, J.A., Lamers, P.P., Martens, D.E., Rinzema, A., Wijffels, R.H. (2013). A model for customising biomass composition in continuous microalgae production. *Bioresour. Technol*., **146**, 89–100.

Koller, A. P., H. Löwe, V. Schmid, S. Mundt and D. Weuster-Botz (2017). Model-supported phototrophic growth studies with *Scenedesmus obtusiusculus* in a flat-plate photobioreactor. *Biotechnol. Bioeng*., **114**, 308-320.

Koren, I., Boussiba, S., Khozin-Goldberg, I., Zarka A. (2021). Chromochloris zofingiensis (Chlorophyceae) divides by consecutive multiple fission cell-cycle under batch and continuous cultivation. *Biol*., **10**, 157.

Krujatz, F., Illing, R., Krautwer, T., Liao, J., Helbig, K., Goy, K., Opitz, J., Cuniberti, G., Bley, T., & Weber, J. (2015). Light-fieldcharacterization in a continuous hydrogen-producing photobioreactor by optical simulation and computational fluid dynamics. *Biotechnol. Bioeng.,* **112**, 2439–2449.

Kumar, A., Ergas, S., Yuan, X., Sahu, A., Zhang, Q., Dewulf, J., Malcata, F.X. and Van Langenhove, H. (2010). Enhanced CO2 fixation and biofuel production via microalgae: recent developments and future directions. *Trends Biotechnol.,* **28**, 371–80.

Kumar, K., Dasgupta, C. N., Nayak, B., Lindblad, P., Das, D. (2011) Development of suitable photobioreactors for CO2 sequestration addressing global warming using green algae and cyanobacteria. *Bioresour. Technol.,* **102**, 4945–4953.

Kumar V., Jain S. (2014). Plants and Algae Species: Promising Renewable Energy Production Source. Emir. *J. Food Agric,* **26**, 679.

Lee E, Jalalizadeh M, Zhang Q. (2015). Growth kinetic models for microalgae cultivation: a review. *Algal Res.* **12**, 497–512.

Lee, H.Y., L.E. Erickson, S.S. Yang (1987). Kinetics and bioenergetics of light-limited photoautotrophic growth of Spirulina platensis. *Biotechnol. Bioeng*., **29**, 832–843.

Lindblad, P., Fuente, D., Borbe, F., Cicchi, B., Conejero, J.A., Couto, N., Čelešnik, H., Diano, M.M., Dolinar, M., Esposito, S. and Evans, C. (2019). CyanoFactory, a European Consortium to Develop Technologies Needed to Advance Cyanobacteria as Chassis for Production of Chemicals and Fuels. *Algal Res.,* **41**, 101510

Lobry, J., Rosso, L., Flandrois, J. (1991). A FORTRAN subroutine for the determination of parameter confidence limits in non-linear models. *Binary,* **3**, 25.

López Muñoz, I., Bernard, O. (2021). Modeling the Influence of Temperature, Light Intensity and Oxygen Concentration on Microalgal Growth Rate. *Processes* **9**, 496.

López-Rosales, L., García-Camacho, F., Sánchez-Mirón, A., Beato, E. M., Chisti, Y., & Grima, E. M. (2016) Pilot-scale bubble column photobioreactor culture of a marine dinoflagellate microalga illuminated with light emission diodes. *Bioresour. Technol*., **216**, 845–855.

Ma, S., Zeng, W., Huang, Y., Zhu, X., Xia, A., Zhu, X., Liao, Q. (2022). Revealing the synergistic effects of cells, pigments, and light spectra on light transfer during microalgae growth: A comprehensive light attenuation model. *Bioresour. Technol.,* **348**, 126777.

Manhaeghe, D., Michels, S., Rousseau, D.P.L., Van Hulle, S.W.H. (2019). A semi-mechanistic model describing the influence of light and temperature on the respiration and photosynthetic growth of Chlorella vulgaris, *Bioresour. Technol*., **274**, 361-370.

Maroneze, M.M., Siqueira, S.F., Vendruscolo, R.G., Wagner, R., de Menezes, C.R., Zepka, L.Q. and Jacob-Lopes, E. (2016). The role of photoperiods on photobioreactors: a potential strategy to reduce costs. *Bioresour. Technol.,* **219**, 493–499.

Mata T.M., Martins A.A., Caetano N.S. (2010). Microalgae for biodiesel production and other applications: a review. *Renew. Sustain. Energy Rev.,* **14**, 217–32.

Metsoviti, M. N., Papapolymerou, G., Karapanagiotidis, I.T., Katsoulas, N. (2020). Effect of light intensity and quality on growth rate and composition of Chlorella vulgaris. *Plants* **9**, 31–17.

Metting, F.B. (1996). Biodiversity and application of microalgae. *J. Ind. Microbiol. Biotechnol.,* **17**, 477–489.

Mohsenpour, S.F., Hennige, S., Willoughby, N., Adeloye, A., Gutierrez, T. (2021). Integrating micro-algae into wastewater treatment: a review. *Sci. Total Environ*., **752**, 142168.

Molina E., Fernández J., Acién F.G., Chisti Y. (2001). Tubular photobioreactor design for algal cultures. J *Biotechnol*., **92**, 113131.

Molina Grima E., Garcia Camacho F., Sanchez Perez J.A., Fernandez Sevilla J.M., Acien Fernandez F.G., Contreras Gomez A. (1994). A mathematical model of microalgal growth in light-limited chemostat culture. *J. Chem. Technol. Biotechnol.,* **61**, 167–73.

Monod J. (1949). The growth of bacterial cultures. *Annu. Rev. Microbiol*., **3**, 371–94.

Muller-Feuga, A., Le Guédes, R., Pruvost, J. (2003). Benefits and limitations of modeling for optimization of Porphyridium cruentum culture in annular photobioreactor. *J. Biotechnol.,* **103**, 153–163.

Neofotis, P., A. Huang, K. Sury, W. Chang, F. Joseph, A. Gabr, S. Twary, W. Qiu, O. Holguin, J. E.W. Polle (2016). Characterization and classification of highly productive microalgae strains discovered for biofuel and bioproduct generation. *Algal Res.,* **15**, 164-178.

Ogbonna, J.C., Yada, H., Tanaka H., (1995). Kinetic study on light-limited batch cultivation of photosynthetic cells. *J. Ferment. Bioeng*., **80**, 259–264.

Packer A, Li Y, Andersen T, Hu Q, Kuang Y, Sommerfeld M. (2011). Growth and neutral lipid synthesis in green microalgae: a mathematical model. *Bioresour. Technol*., **102**, 111–7.

Płaczek, M.; Patyna,A.; Witczak, S., (2017). Technical evaluation of photobioreactors for microalgae cultivation. *E3S Web of Conferences,* **19**, 02032.

Pruvost J. (2019). Cultivation of algae in photobioreactors for biodiesel production. In: *Biofuels: Alternative Feedstocks and Conversion Processes for the Production of Liquid and Gaseous Biofuels*. (Second Edition). Academic Press, London (UK), 629-659.

Ras, M., Steyer, JP. & Bernard, O. (2013). Temperature effect on microalgae: a crucial factor for outdoor production. *Rev. Environ. Sci. Biotechnol.,* **12**, 153–164.

Rizwan, M., Mujtaba, G., Memon, S.A. , Lee, K., Rashid, N. (2018). Exploring the potential of microalgae for new biotechnology applications and beyond: a review, Renew. Sustain. Energy Rev. **92**, 394-404.

Ross, B.S., Pott, R.W.M. (2022). Investigating and Modeling the Effect of Light Intensity on *Rhodopseudomonas Palustris* Growth. *Biotechnol. Bioeng.,* **119**, 907–921.

Rubio, F.C., Camacho, F.G., Sevilla, J.M., Chisti, Y., Grima, E.M. (2003). A mechanistic model of photosynthesis in microalgae. *Biotechnol. Bioeng*., **81**, 459–473.

Salama, E.S., Kurade, M.B., Abou-Shanab, R.A., El-Dalatony, M.M., Yang, I.S., Min, B., and Jeon, B.H., (2017). Recent progress in microalgal biomass production coupled with wastewater treatment for biofuel generation. *Renew. Sustain. Energy Rev*., **79**, 1189–211.

Schuster, A. (1905). Radiation through a foggy atmosphere. *Astrophys. J.,* **21**, 1.

Sforza, E., Pastore, M., Franke, S. M., & Barbera, E. (2020). Modeling the oxygen inhibition in microalgae: An experimental approach based on photorespirometry. *New biotechnol*., **59**, 26-32.

Sforza, E., Pastore, M., Barbera, E., & Bertucco, A. (2019). Respirometry as a tool to quantify kinetic parameters of microalgal mixotrophic growth. *Bioprocess Biosyst. Eng*., **42**, 839-851.

Sheng, B., Fan, F., Huang, J., Bai, W., Wang, J., Li, S., Li, W., Wan, M., Li, Y., (2018). Investigation on models for light distribution of Haematococcus pluvialis during astaxanthin accumulation stage with an application case. *Algal Res.,* **33**, 182 –189.

Solimeno, A., Samsó, R., Uggetti, E., Sialve, B., Steyer, J.P., Gabarró, A., García, J. (2015). New mechanistic model to simulate microalgae growth. *Algal Res.,* **12**, 350–358.

Steele JH. (1962). Environmental control of photosynthesis in the sea. *Limnol. Oceanogr.,* **7**, 137–50.

Sun H, Kong Q, Geng Z, Duan L, Yang M, Guan B. (2015). Enhancement of cell biomass and cell activity of astaxanthin-rich Haematococcus pluvialis. *Bioresour Technol.*, **186**, 67–73.

Sztretye M., Dienes B., Gonczi M., Czirjak T., Csernoch L., Dux L., Szentesi P., Keller-Pinter A. Astaxanthin: A Potential Mitochondrial-Targeted Antioxidant Treatment in Diseases and with Aging. *Oxid. Med. Cell. Longev*, **2019**, 1-14.

Talbot, P., J.M. Thébault, A. Dauta, J. De la Noüe (1991). A comparative study and mathematical modeling of temperature, light and growth of three microalgae potentially useful for wastewater treatment. *Water Res.,* **25**, 465–472.

Tamiya, H., Hase, E., Shibata, K., Mituya, A., Iwamura, T., Nihei, T. (1953). Kinetics of growth of Chlorella, with special reference to its dependence on quantity of available light and on temperature. *Algal. Cult. Lab. Pilot. Plant.,* 204–32.

Torzillo, G., Zittelli, G.C. (2015). Tubular Photobioreactors. In: *Algal Biorefineries*. Springer, Cham (CH), 187-212.

Van Oorschot, J.L.P. (1955). Conversion of Light Energy in Algal Culture. *PhD diss.,* Wageningen University.

Vieira, M.V.; Pastrana, L.M.; Fuciños, P. (2020). Microalgae Encapsulation Systems for Food, Pharmaceutical and Cosmetics Applications. *Mar. Drugs,* **18**, 644.

Wágner, D.S., Valverde-Pérez B., Plósz, B.G. (2018). Light attenuation in photobioreactors and algal pigmentation under different growth conditions – model identification and complexity assessment. *Algal Res.,* **35**, 488-499.

Wang B., Lan C.Q, Horsman M. (2012). Closed photobioreactors for production of microalgal biomasses. *Biotechnol.Adv.,* **30**, 904-912.

Wood, E. E., Ross, M. E., Jubeau, S., Montalescot, V., & Stanley, M. S. (2022). Progress towards a targeted biorefinery of Chromochloris zofingiensis: a review. *Biomass Conv. Bioref*., 1-26.

Yaakob M.A., Mohamed R.M.S.R., Al-Gheethi A., Ravishankar G.A., Ambati R.R. (2021). Influence of nitrogen and phosphorus on microalgal growth, biomass, lipid, and fatty acid production: An overview. *Cells*, **10**, 393.

Zhang, C., Chen, X., Too, H.P. (2020). Microbial astaxanthin biosynthesis: recent achievements, challenges, and commercialization outlook. *App. Microbiol. Biotechnol*., **104**, 5727–5737.

Zhang, Y., Ye, Y., Bai, F., & Liu, J. (2021). The oleaginous astaxanthin-producing alga Chromochloris zofingiensis: potential from production to an emerging model for studying lipid metabolism and carotenogenesis. *Biotechnol. Biofuels*, **14**, 119.

Zhu S., Huang W., Xu J., Wang Z., Xu J., Yuan Z. (2014). Metabolic changes of starch and lipid triggered by nitrogen starvation in the microalga Chlorella zofingiensis. *Bioresour. Technol.*, **152**, 292–298.

Zittelli, G. C., Biondi, N., Rodolfi, L., Tredici, M. R., (2013). Photobioreactors for mass production of microalgae. In: *Handbook of Microalgal Culture*. (Second Edition). John Wiley & Sons, Hoboken (US), 225–266.

Websites

Cell-DEG GmbH (2023). *Products*. URL: https://celldeg.com/products/product-family/. Last access: 05/07/2023.

Puevit GmbH (2023). *Products*. URL: https://puevit.com/building-integrated-algae-farms/. Last access: 10/07/2023.